NEW YORK UNIVERSITY
WASHINGTON SQUARE
NEW YORK, NEW YORK 10021

A SCALE MODEL WIND TUNNEL STUDY OF DISPERSION IN THE CLEVELAND AREA - LABORATORY SIMULATION OF LAKE BREEZE EFFECTS ON DIFFUSION FROM GROUND LEVEL EMISSIONS

FINAL REPORT

FOR

NATIONAL AERONAUTICS AND SPACE ADMINISTRATION

GRANT NGR-33-016-197

FEBRUARY 1973 - MARCH 1974

WALTER G. HOYDYSH
PRINCIPAL INVESTIGATOR

ABSTRACT

A wind tunnel simulation of the diffusion patterns in a sea breeze has been attempted. No attempt was made to reproduce the recirculation that characterizes a sea breeze, but the results indicate that the low level onshore flow was well simulated for neutral, stable, unstable, and elevated inversion conditions. Velocity, turbulence, shear stress, and temperature data were taken, and the spread of emissions from ground level sources was investigated.

Comparison is made with theoretical predictions by E. Inoue and with the open, homogeneous plane field results of Pasquill. Agreement with the predictions by Inoue is good. The comparison with Pasquill's results shows that the wind tunnel flows are shifted two categories towards more stable. The discrepancy may be explained as a matter of averaging time.

1. INTRODUCTION

Near large bodies of water, sea breezes (or lake breezes) are common features of the climatology. The different surface temperature and roughness between sea and land causes complicated stratification of the air flow, which tends to create an elevated inversion. This causes fumigation and plume trapping (Lyons and Cole, 1973). This and the occurrence of return flow make the sea breeze an important factor when studying the dispersion of pollutants near lake or sea shores where large industries are commonly situated.

Figure 1 is a schematic diagram showing the flow patterns commonly occurring in a sea breeze. The height of the boundary layer above the sea may be 300m to 400m The sea breeze flows from 5km to as much as 40km inland, and then rises, forming a front. The flow then reverses and returns seaward at a height of 600m or more, usually not exactly 180° to the onshore flow. It may then gradually descend and flow onshore again, making a complete cycle. Within the sea breeze, the velocity and temperature profiles change continuously since the roughness and temperature on the land surface are different from those of the sea surface.

Yoshida, Aoki and Takamatsu (1972) found that the sea breeze advances as a wedge near the ground and the diffusivity may become very small in this wedge. Fukuoka (1968) investigated high concentrations occurring upwind from a stack. Such occurrences may be explained by the return flow which feeds pollutants to the sea breeze as it invades the land. Lyons (1970) observed a similar return of pollutant at lake

Michigan. Wakamatsu, et al. (1971) found SO_2 concentrations behind a sea breeze front five to ten times higher than the concentrations before the sea breeze began. After the sea breeze died, concentrations returned to the morning values. Nakano (1972) observed a similar variation of concentration during the sea breeze cycle.

With current techniques it is not yet possible to simulate the complete sea breeze, including return flow in the wind tunnel. The experiment reported here is an attempt to simulate the surface layer flow and to study the gross flow characteristics -- mean velocity, turbulence, and temperature profiles -- and the concentration dispersion patterns for ground level sources located on the land under the influence of thermal stratification.

2. THE WIND TUNNEL MODEL

The typical surface boundary conditions of the sea breeze might be described as follows:

sea: small roughness length (z_{os}), lower surface temperature (θ_s)

land: large roughness length ($z_{o\ell}$), and/or elevated topography, higher daytime surface temperature (θ_ℓ).

These conditions also describe suburban and urban areas respectively, so similar conditions may be used to simulate both sea breeze and urban heat island effects on diffusion.

The turbulent boundary layers in the actual and model sea breezes may be compared using the turbulent Reynolds number and densimetric Froude number. The turbulent Reynolds number at height H is

$$Re_{turb} = \frac{U(H)\ H}{K(H)}$$

where K is the turbulent diffusion coefficient (eddy diffusivity). If a logarithmic wind profile is assumed, then $K(H) = ku_*H$ and

$$Re_{turb} = \frac{\frac{u_*}{k}\ln\left(\frac{H}{z_o}\right) H}{ku_*H} = \frac{1}{k^2}\ln\left(\frac{H}{z_o}\right)$$

which does not depend on the wind velocity but only on the roughness length.

Generally, z_o and the boundary layer thickness, δ, over the sea are about 10^{-1} cm and 350 m respectively; therefore, $Re_{turb} = 80$. If $\delta = 15$ cm in the wind tunnel, then $z_o = 5 \times 10^{-5}$ cm is required to simulate the above

turbulent Reynolds number. By similar reasoning, $z_o = 5 \times 10^{-3}$ cm would be required for the land portion of the model. Both values were too small to be achieved in the wind tunnel, where $z_o = 5 \times 10^{-2}$ cm was obtained by using smooth aluminum plates. Most of the mechanical turbulence comes from large scale local geometry rather than roughness length. For this experiment, it was decided that large scale geometry such as topography could be simulated by elevating the land 1.25 cm above the sea.

Using the densimetric Froude number as a criterion for simulating the temperature differences (Snyder (1972), Cermak (1971), McVehil, Ludwig and Sundaram (1967)),the following temperature difference is required:

$$\left(\frac{\Delta\theta}{\theta}\right)_m = \left(\frac{\Delta\theta}{\theta}\right)_p \left(\frac{U_m}{U_p}\right)^2 \frac{H_p}{H_m}$$

where m and p refer to model and prototype. $\Delta\theta$ is characteristic temperature difference, taken here as the sea (θ_s) and land (θ_l) difference. For $\Delta\theta_p = 5°$ C, $U_p = 5$ m/s, $U_m = 1$ m/s, and $H_p/H_m = 2000$ (an approximate value which equates the 1.25 cm step with a 24 m topography change), then $\frac{\Delta\theta_p}{\Delta\theta_m} = \frac{1}{80}$ is required, meaning a wind tunnel floor temperature difference of about 400° C, an impossible condition.

In a flow field with both mechanical and thermal turbulence, the two influence each other. A surface to air temperature gradient changes turbulent components and these influence the mean velocity profile and turbulent diffusion coefficient. These in turn alter the temperature profile. Thus, the temperature and velocity fields are not independent. In this sense, Richardson number, a ratio of mechanical to thermal energy, becomes important for diffusion phenomena in thermally stratified fields.

Four surface temperature conditions were considered in this study, corresponding to neutral, unstable, stable and elevated inversion conditions. A maximum of $\Delta\theta = 30°$ C was chosen as the sea-land surface temperature difference. This is small compared with the required temperature difference from Froude number, however, a large vertical temperature gradient above the ground created Richardson numbers the same order of magnitude as might be expected in the atmosphere, although for short downwind distances.

The gradient Richardson number is given as

$$Ri = \frac{g \frac{\partial \theta}{\partial z}}{\theta_o \left(\frac{\partial U}{\partial z}\right)^2}$$

Minus values indicate unstable conditions, plus values indicate stable conditions. If $|Ri|$ is nearly zero, mechanical turbulence dominates, whereas a large $|Ri|$ shows that thermal turbulence dominates.

The relation between L (Monin - Obukov length) and Ri can be shown to be:

$$Ri = \frac{z}{L} \frac{\alpha}{\phi_m}$$

where α is the ratio of turbulent diffusion coeffients of momentum and heat and ϕ_m is a nondimensional shear term.

The mean velocity profile for near neutral conditions is given by:

$$U = \frac{u_*}{k} \ln \left(\frac{z}{z_o} \right) + \beta \frac{z}{L}$$

which is the so called log-plus-linear law, where β is a constant. For unstable conditions, L is less than zero, making plots of log z vs U concave upwards. For stable conditions, L is greater than zero, so the semi-log velocity curves become concave down.

If the sea is colder than the air above it, the air over the water becomes stably stratified. As this air moves over the land, it is heated from below by the land, and the stratification near the ground changes to unstable. Therefore, the vertical profile of the Richardson number changes from minus to plus with increasing height. The height where Ri = 0 corresponds to the height of the base of the inversion which develops. Thus the Richardson number profile can be important and useful for describing the flow and diffusion fields.

3. DIFFUSION UNDER NON-NEUTRAL CONDITIONS

Many of the presently used diffusion equations do not appropriately describe diffusion in the atmosphere under non-neutral conditions. Empirical theories, such as Pasquill's, work well under non-neutral conditions over a homogeneous plane, but are difficult, if not impossible, to apply in the case of a sea breeze. Such theories, designed for constant conditions in x and y, typically cannot account for the longitudinal variation of stability that occurs in a sea breeze.

The results obtained from this experiment will be compared with several useful relations developed by E. Inoue (1960). Inoue considered three conditions: extremely unstable, neutral and extremely stable and found the following approximate relations for σ_y, σ_z and the ground level concentration as functions of downwind distance:

extremely unstable	σ_y	$\propto$	x
	σ_z	$\propto$	$x^{1.5}$
	$C_{z=0}$	$\propto$	$x^{-2.5}$
neutral	σ_y	$\propto$	x
	σ_z	$\propto$	$x^{0.8}$
	$C_{z=0}$	$\propto$	$x^{-1.8}$
extremely stable	σ_y	$\propto$	x
	σ_z	$\propto$	$x^{0.5}$
	$C_{z=0}$	$\propto$	$x^{-1.5}$

These relations may be used in a step-by-step method in comparison with experimental results for flows with changing stability. As stability changes with distance from the shoreline, the appropriate power relation changes. Log-log graphs of the experimental results can therefore be used to indicate the stability category and the approximate strength of the stability.

4. EXPERIMENTAL APPARATUS AND MEASUREMENT TECHNIQUE

The tests were performed in the Air Pollution Wind Tunnel at New York University. The wind tunnel test section is 1.1 m x 2.2 m x 10 m (3.5 ft. x 7 ft. x 35 ft.) and has heaters for controlling the air intake temperature and maintaining the same wall, floor and ceiling temperatures. A survey carriage allows the remote positioning of probes to the nearest 0.25 mm.

The model for this experiment consisted of six smooth aluminum plates providing 365 cm of "sea" and 365 cm of "land". The sea portion was raised 2.5 cm from the wind tunnel floor so that the step would generate a turbulent boundary layer). The land portion was raised an additional 1.25 cm for topographic similarity, as discussed earlier. Twelve heating tapes with separate controllers were fastened to the underside of the land surface to provide temperatures up to 100° C with good uniformity. The sea surface was cooled by slipping slabs of dry ice into the space between the aluminum plates and the wind tunnel floor. Flush mounted, 2.5 cm diameter sources covered with stainless steel mesh were added to the land at downwind distances of 2.5, 25 and 100 cm from the step between the sea and land. Sixteen thermocouples were fastened to the upper surface to be used for recording and adjusting the surface temperature. The resulting configuration is shown in Figure 2.

Velocity data were measured and recorded using a DISA constant temperature anemometer system. Mean velocity, vertical and longitudinal turbulent velocities, Reynolds stress and heat flux were determined by a procedure described by Arya (1968). This technique involves rotating a

single hot wire , so a probe rotater was constructed to turn the probe support about its long axis in precise 45° intervals. A fine gage thermocouple and a resistance thermometer were also fastened to the rotater to measure temperature profiles and the r.m.s. of the temperature fluctuations.

The sources built into the land were fed a mixture of 2% ethane in nitrogen. This hydrocarbon tracer was sampled from a single brass probe on the survey carriage using a Beckman hydrocarbon analyzer. The output was recorded and time-averaged with one minute averaging.

5. DISCUSSION OF RESULTS

5-1. Flow Measurements

The following graphs summarize the flow data in nondimensionalized form for the four test conditions with crossplots for comparison. All distances are nondimensionalized by the step height ($d = 1.25$ cm), $x^* = x/d$ is the nondimensional downwind distance from the step at the sea-land interface, and $z^* = z/d$ is the local nondimensional height above the plates, except in the plot of log z^* vs. U^* (Figure 3d), where z^* is measured from sea level. Wind speed, turbulent velocities and Reynolds stress are nondimensionalized using the free stream velocity $U_\infty = 1.0$ m/s. Temperatures are plotted in Centigrade degrees over or under wind tunnel ambient, 30° C. The labels Neutral, Unstable, Stable and Inversion are applied in a generic sense to simplify the description of the wind tunnel conditions.

The flow characteristics were measured for all four stability categories, but complete data for only the Inversion case are presented here for the sake of brevity. Figure 3 shows the nondimensionalized mean velocity, the mean temperature and the Richardson number profiles for the Inversion case. The results illustrate the characteristics of a typical elevated inversion. The velocity profiles in Figure 3a show the rapid readjustment which occurs downwind of a step in a flow field. In Figure 3b the temperature gradient is unstable below the inversion base and stable above the base.

The Richardson number profiles show the inversion details more clearly. Richardson number was calculated using the data contained in Figures 3a and 3b and the gradient form

$$Ri = \frac{g \frac{\partial \theta}{\partial z}}{\theta_a \left(\frac{\partial U}{\partial z}\right)^2}$$

The Richard numbers have a wide range, so a logarithmic scale has been used in Figure 3c with an overlap at $Ri = \pm 10^{-3}$. The height where $Ri = 0$ corresponds to the elevation of the inversion base. The height of the inversion base increases almost linearly with downwind distance. The semi-log velocity profiles, Figure 3d, have the characteristics predicted by the log-plus-linear law of Monin and Obukhov. In the unstable layer below the inversion, the profiles appear concave down and reverse to be concave upward in the stable layer above the inversion base. Using the inflection points where the concave up and down portions meet as an indication of the inversion height, it may be seen that this prediction yields approximately the same heights as does the Richardson number profile.

Figure 4 shows comparisons of the Neutral, Unstable, Stable and Inversion flow data at $x^* = 20$. In Figure 4a, which shows mean velocity profiles, it may be seen that the Neutral and Unstable boundary layer thicknesses are approximately the same, but the Unstable profile shows increased velocity at lower height due to increased vertical turbulence, which augments momentum transfer from higher to lower levels. The Stable and Inversion boundary layer thicknesses are smaller, with less uniform velocity.

Figure 4b shows the corresponding mean temperature profiles for the Unstable, Stable and Inversion conditions. The unstable layer thickness is $z^* < 4$. The stable layer thickness is $z^* < 8$, considerably greater than the unstable layer because the stable layer was developed over an additional 365 cm of upwind "sea". The Inversion case temperature profile is unstable for $z^* < 2$ and stable for $2 < z^* < 8$.

Longitudinal turbulence ($\sqrt{\overline{u^2}}$), vertical turbulence ($\sqrt{\overline{w^2}}$), and Reynolds stress ($-\overline{uw}$) are smallest for the Stable case flow and greatest for the Unstable case, as shown in Figures 4 c, d, and e. Neutral cases values typically fall between the Stable and Unstable values. Inversion case values are close to the Stable for $2 < z^* < 8$, and closer to the Unstable case values for $z^* < 2$. Figure 4f shows that the vertical heat flux is a small minus value for the Stable case flow and a large plus value for the Unstable flow. The heat flux for the Inversion case is a small minus value in the stable layer above the inversion base and a large plus value in the unstable layer below the base.

5-2. Concentration Measurements

Concentration measurements were carried out for the four air stabilities (Neutral, Unstable, Stable and Inversion) and three different ground level source locations. For each of these twelve cases, ground level crosswind profiles and vertical profiles were determined at five downwind distances from the source. Distances have been nondimensionalized by the step height as per the velocity data. The sources are designated simply No. 1, No. 2, and No. 3 at nondimensional distances of 2, 20 and 80, respectively from the step (shoreline). Except where the omission would neglect important details only data concerning Source No. 2 is presented here. For each source, $x^{*\prime}$ signifies the distance from the center of the source, in order to simplify comparison. The concentrations were normalized by the concentration measured at the downwind edge of the 2.5 cm. diameter source. These are multiplied by 10^3 for convenience.

Figure 5 shows the vertical concentration profiles at four downwind positions from Source No. 2 for the four stability conditions. In general, the Unstable profiles have the greatest spread, followed by Neutral, Inversion and Stable. On the other hand ground level concentrations generally were highest for Stable, followed by Inversion, Neutral and Unstable as a consequence of the different spreads.

Figure 6 shows the vertical profile at $x^{*\prime} = 20$ for source No. 2 with greater detail. The Neutral case profile has almost a linear decrease with increasing height for the semi-log coordinates shown indicating an exponential decay. The Unstable case profile also appears exponential,

however, another point off the graph (the trend is indicated by the line) and the profiles at other $x^{*\prime}$ positions show that the curve is not exponential. The Stable and Inversion case profiles are both considerably compressed; the Inversion case is slightly less so because of the unstable layer below the inversion base. These compressions correspond to the decreased vertical turbulence near the ground as shown in Figure 4d.

Vertical standard deviations (σ_z), defined as the second moment of the profile about its mean were calculated for each profile. The values of σ_z were nondimensionalized by the step height and are presented in Figure 7. Data from Source No. 1 have been included because they show details which became obscured downwind of Source No. 2, where the inversion became weaker. The values of σ_z are largest for the Unstable condition, and decrease for Neutral and Stable. The three slopes indicated at the bottoms of the graphs correspond to the predicted increases for extremely unstable ($x^{3/2}$), neutral ($x^{0.8}$) and stable ($x^{1/2}$). The experimental Stable results have a smaller slope than predicted, and the Unstable and Neutral have slightly smaller slopes than predicted. Since Source No. 1 was near the step, where heating had just begun, it may be expected that the unstable stratification would be weak, and the stable would be strong, because the source was close to the sea. The new internal boundary layer created by the step might be expected to affect σ_z, but the changes due to stability appear to be more significant. It is interesting to note that the Inversion σ_z has almost the same value as the Stable σ_z , but increases rapidly to the Neutral and Unstable values. Since the flow is predominantly

stable near Source No. 1, and the unstable layer underneath becomes thicker with distance, such a rapid increase is reasonable.

Figure 7b shows that the characteristics for Source No. 2 were generally the same as for Source No. 1, with the expected changes that accompany the greater distance. The trapping of the plume by the inversion layer can be seen more clearly in Figure 8, which shows the heights at which the concentrations equal one-tenth of the peak concentrations for each source under the inversion condition. The heavy dashed line corresponds to the height of inversion base according to the Richardson number profiles. The plume boundary height from Source No. 1 is almost the same as the inversion height which suggest trapping due to the stable layer above this height. The plume boundary for the Neutral case is higher close to the source but lower farther downwind. The plume boundaries from Source No. 2 are almost the same under Neutral and Inversion conditions, while the height under Inversion conditions is greater than under neutral for Source No. 3. At these downwind locations, the unstable stratification under the inversion raises the plume boundary higher than it was for the neutral case.

Figure 9 shows ground level crosswind profiles at four downwind distances from Source No. 2 under the Neutral, Unstable, Stable and Inversion conditions. As already shown by the vertical profiles the magnitude of the ground level concentrations on the centerline depends on stability with the same relationship of Stable as highest and Unstable lowest.

The spreads also follow the same pattern: widest for Unstable and Neutral and narrowest for Stable.

The crosswind profiles can be accurately described by normal distributions. The standard deviations σ_y were determined by plotting the nondimensional concentrations on probability paper, from which the standard deviation and location of the mean can be read easily. Because 2.5 cm diameter sources were used in this study, σ_y does not fall to zero at $x^{*\prime} = 0$, but had a value of $\sigma_y = 0.75$ cm. This is reasonable if a normal distribution is accounted at the source position. To convert the area source data to point source data for comparison with field studies, $\sigma_y = 0.75$ cm. has been subtracted from the wind tunnel values. These values of σ_y have then been nondimensionalized using the step height to obtain $\sigma_y^* = \sigma_y/d$.

Figure 10 shows plots of the log of these converted σ_y^* values versus x^*, for Sources No. 1 and 2. In each case, the curves show that $\sigma_y^* \propto x^1$, approximately. Unstable values of σ_y^* are largest, followed by Neutral and Stable, the same relations as for σ_z^*. For Source No. 1 the Inversion σ_y^* also begins at a small value, the same as Stable, and increases to a value greater than the Neutral value., However, for Source No. 2, the Inversion σ_y^* are much closer to the Unstable values, as was the case for σ_z^*.

Figure 11 shows the centerline ground level decays of concentration with downwind distance for Sources No. 1 and 2. According to Inoue

(1969), the ground level concentrations may be proportional to $x^{-1.5}$ for extremely stable, $x^{-1.8}$ for neutral, and $x^{-2.5}$ for extremely unstable. These slopes are drawn in the figure for comparison. For both sources, the agreement between predicted and experimental results is good except for Source No. 1 at the smaller values of $x^{*\prime}$, which may be due to step effects.

5-3. Comparison with Field Diffusion Experiments

Most recent field experiments have been compared with Pasquill's six stability categories, and the agreement for the available experimental data over flat, homogeneous planes is quite good. But near the seashore, where sea or land breezes occur frequently, these curves will not always fit the results of field diffusion experiments.

Using data from their field experiment near the seashore, Sakuraba et al. (1967) plotted calculated values of σ_y over Pasquill's curves. These were shifted two categories in the stable direction, and, if the longer sampling time were accounted for (30 min. vs. 10 min. for Pasquill's curves), the shift would become even more significant.

Other field studies conducted near the sea show a gradual shift of σ_z from stable category F to neutral category D with distance. Such results show that near the seashore the flow is not homogeneous in the longitudinal direction as it is over open, flat land, where Pasquill's curves were established.

To compare this wind tunnel data with Pasquill's curves, scaling is required. Scales of 1000:1, 2000:1 and 3000:1 were investigated when recalculating the wind tunnel data for comparison with Pasquill's curves. At 1000:1, the data points spread from x = 125 to 1000 meters. Increasing the scale ratio increased this distance and shifted stability class from stable towards neutral. The effect, however, was small, so 2000:1 will be considered an acceptable, representative scale for this comparison.

Figure 12 shows σ_z vs. x for source No. 3 at the scale ratio 2000:1 for the four stability classes tested. The data extends over the range 250

to 2000 meters. The Stable condition curve falls into category F, Neutral into E and Unstable into C to D. At the source location, Inversion values lie between Neutral and Unstable due to the unstable surface layer.

Figure 13 shows σ_y vs. x for Source No. 3 at the scale ratio 2000:1 for the four stability classes. Wind Tunnel Neutral fits F, Unstable fits E, and Stable is much more stable than F. The wind tunnel limits horizontal eddy size, which increases with observation time in the field. Because of the plume meandering the mean concentrations decrease with increased sampling time.

Hino (1966) proposed a 1/2 power decay of σ_y with observation time. This was determined from turbulent diffusion theory and agrees well with experiment for long sampling time (several minutes to several hours).

The wind tunnel data, when multiplied by 2.5, agree well with Pasquill's curves. As Pasquill's curves are for 10 minutes samples, the 1/2 power law then implies that the equivalent wind tunnel sampling time is 1.6 minutes or 96 seconds. This means that the wind tunnel sampling time corresponds to a small observation time for diffusion phenomena in the field .

The normalized centerline ground level concentration used by Pasquill is:

$$\frac{C\,\bar{U}}{Q} = \frac{1}{\pi\,\sigma_y\,\sigma_z}$$

For ground level releases and measurements like those made in this study the value of $\bar{U}$ is difficult to define. Since σ_y and σ_z were measured in the wind tunnel, the normalized concentrations were estimated from these.

Figure 14 shows the normalized ground level concentration, based on the calculated σ_y and σ_z, plotted over Pasquill's curves. A scale ratio of 2000:1 and Source No. 3 were used for the comparison. The results again show a shift of two categories towards stable.

6. CONCLUSIONS AND FUTURE STUDY

Sea breeze effects on diffusion were simulated in the wind tunnel by heating and cooling the wind tunnel floor. Flow and diffusion characteristics were measured for four stabilities. Close to the shoreline, stable or inversion conditions increased the ground level concentrations behind the ground level sources to more than five times the neutral values. Since most wind tunnel diffusion studies have been carried out for neutral stability, this result is especially significant. Inflow of stable air from a sea or lake is a common part of the climatology for seaside industrial parks, so stability effects due to sea breezes are important to air quality.

In the present study, diffusion from a ground level source was considered. For a more realistic study, an elevated source model is desirable. Such a study will be next in the series of thermal experiments being conducted by the authors. The relation of source height to inversion layer height would be very important in a study of fumigation, where higher ground level concentrations may be expected than would occur for an elevated source with neutral conditions.

Acknowledgement

The Environmental Research Laboratories of New York University gratefully acknowledge the support of the Lewis Research Center of the National Aeronautics and Space Administration (NGR 33-016-197), under whose sponsorship this work was carried out.

REFERENCES

Arya, S.P.S.: 1968, 'Structure of Stably Stratified Turbulent Boundary Layer', Fluid Dynamics and Diffusion Laboratory, Colorado State University. CER 68-69 SPSA 10.

Cermak, J.E., : 1971, 'Laboratory Simulation of the Atmospheric Boundary Layer', AIAA Journal, Vol. 9, No. 9. pp 1746-1754

Fukuoka, Y.: 1968, 'High Concentration Upwind of the Pollutant Source'. Report, Chiba Air Pollution Control Laboratory. (In Japanese).

Hino, M.: 1968, 'Maximum Ground Level Concentration and Sampling Time', Atmospheric Environment, 2, 149.

Inoue, E.: 1960, 'Studies of the Diffusion Phenomena in the Atmospheric Surface Layer, Part 1. Diffusion of Smoke from a Continuous Fixed Source on the Ground Surface'. Agriculture Meteoro. Japan Vol. 16 No. 2 (In Japanese).

Lyons, W.A.: 1972, 'Mesoscale Transport of Pollutant in the Chicago Area as Affected by Land and Lake Breezes', Proc. 2nd Intern. Clean Air Congress, New York, Academic Press.

Lyons, W.A., and H.S. Cole: 1973, 'Fumigation and Plume Trapping on Shores of Lake Michigan During Stable Onshore Flow'. J. Appl. Meteor., 12, 494-510

McVehil, G.E., G.R.Ludwig and T.R. Sundaram.: 1967, 'On The Feasibility of Modeling Small Scale Atmospheric Motions'. CAL Report No. ZB-2328-P-1.

Monon, A.A., and A.M. Obukhov : 1954, 'Fundamental Regularities of Turbulent Agitation in the Ground Layer of the Atmosphere', Tr. Geojiz, Inst., Ahad. Nank. SSR, Sb24. 163-167.

Nakano, M., H. Takeuchi, Y. Mitsuda, and Fuwa: 1972, 'Meteorological Survey of Air Pollution in Osaka City', J. Japan Society of Air Pollution, Vol. 7, No. 2 (In Japanese)

Ogawa, Y. 1973, 'Effects of Buildings and Thermal Boundary Layer on Diffusion', Ph. D. dissertation, University of Hokkaido.

Ogawa Y., W.G. Hoydysh and R. Griffiths, 1973, 'A Laboratory Simulation of Sea Breeze Effects', New York University Environmental Research Laboratory TR 115

Snyder, W. H.: 1972, 'Similarity Criteria for the Application of Fluid Models to the Study of Air Pollution Meteorology', Boundary Layer Meteorology 3 - 113-134.

Wakamatsu, S., S. Saiki, and S. Kanno: 1971, 'Meteorological Studies on the Air Pollution of Keihin Industrial Region in Winter', J.Japan Society of Air Pollution Vol. 6, No. 1 (In Japanese)

Yoshida, T., J. Aoki, and Y. Takamatsu,: 1972, 'The Relation between Sea Breeze and Air Pollution in Tomakomai Youfutsu', The Proceedings of 1972 Annual Meeting of the Japan Meteorological Association.

Figure 1. Sketch of commonly occuring sea breeze flow patterns.

Figure 2. Schematic of the model. The vertical scale is exaggerated to show the step. A summary of the boundary temperature conditions is given beneath the sketch.

Figure 3. Summary of the downwind development of the measured flow characteristics for the inversion condition.
(a) Nondimensionalized mean velocity profiles
(b) Mean temperature profiles
(c) Richardson number profiles, showing inversion height (dashed line)
(d) Semi-log mean velocity profiles

Figure 4. Comparison of the measured flow characteristics for each stability condition.
(a) Mean velocity profiles
(b) Mean temperature profiles
(c) Longitudinal turbulent intensity
(d) Vertical turbulent intensity
(e) Nondimensionalized Reynolds stress
(f) Vertical heat flux

Figure 5. Summary of the downwind development of the vertical concentration profiles for each stability condition. Source No. 2.

Figure 6. Comparison of the vertical concentration profiles at $x^{*\prime} = 20$ for the four stability conditions. Source No. 2

Figure 7. Vertical standard deviations of the plume spread vs. downwind distance from the source.
(a) Source No. 1
(b) Source No. 2

Figure 8. Plume width for the Neutral and Inversion conditions vs. downwind distance.

Figure 9. Summary of the development of the ground level crosswind concentration profiles for the four stability conditions. Source No. 2.

Figure 10. Crosswind standard deviations of the plume spread vs. downwind distance from the source.
(a) Source No. 1
(b) Source No. 2

Figure 11. Decay of the center line ground level concentration with downwind distance from the source.
(a) Source No. 1
(b) Source No. 2

Figure 12. Comparison of wind tunnel results for σ_z with Pasquill's curves. The wind tunnel data have been multiplied by a scale ratio of 2000:1, as explained in the text.

Figure 13. Comparison of wind tunnel results for σ_y with Pasquill's curves. The wind tunnel data have been multiplied by a scale ratio of 2000:1 , as explained in the text.

Figure 14. Comparison of normalized ground level concentration in the wind tunnel with Pasquill's curves. The wind tunnel data have been multiplied by a scale ratio of 2000:1, as explained in the text.

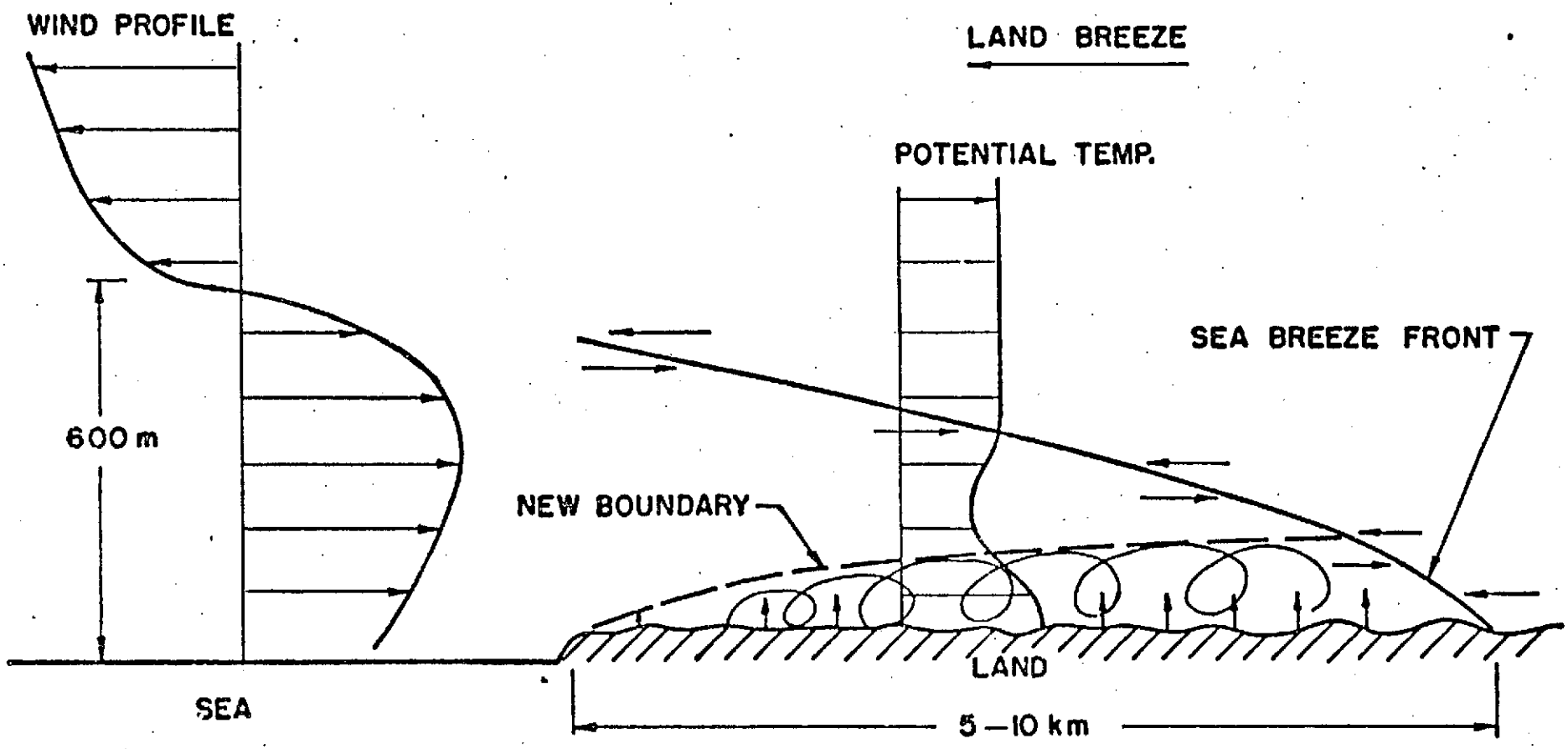
WIND PROFILE
LAND BREEZE
POTENTIAL TEMP.
600 m
SEA BREEZE FRONT
NEW BOUNDARY
LAND
SEA
5—10 km

Figure 1

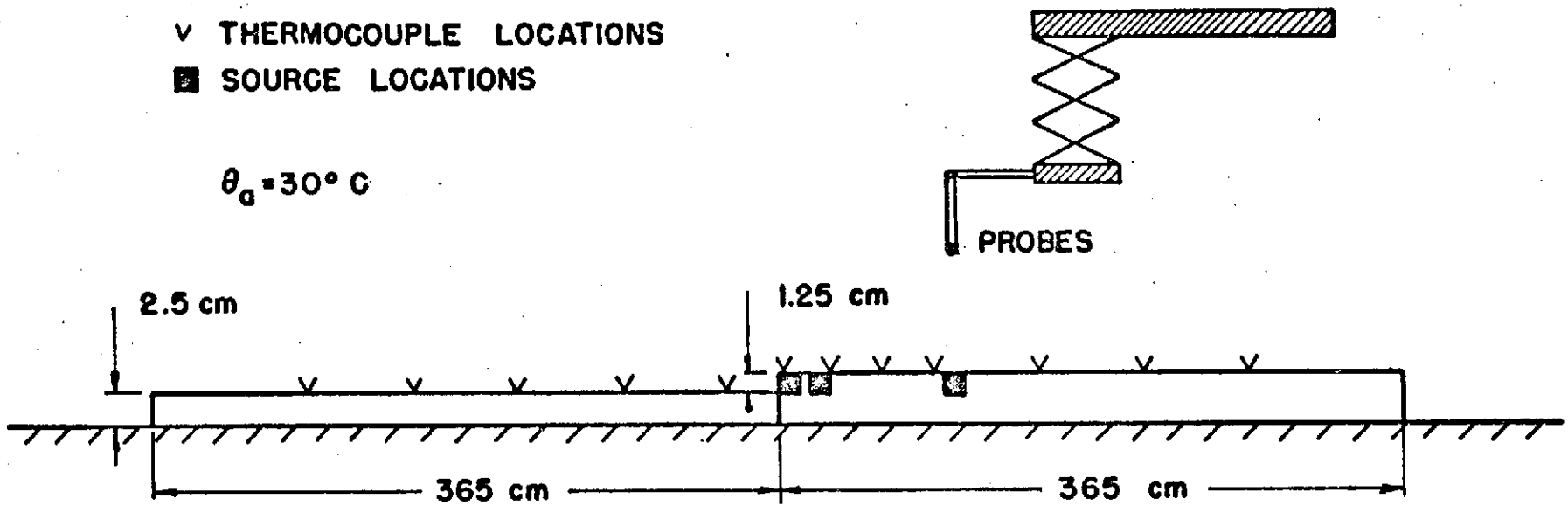

	θ_s °C	θ_l °C
NEUTRAL	30°	30°
UNSTABLE	30°	60°
STABLE	15°	UNHEATED, 28° TO 30°
INVERSION	15°	45°

Figure 2

3o) MEAN VELOCITY

INVERSION (U/U_∞)

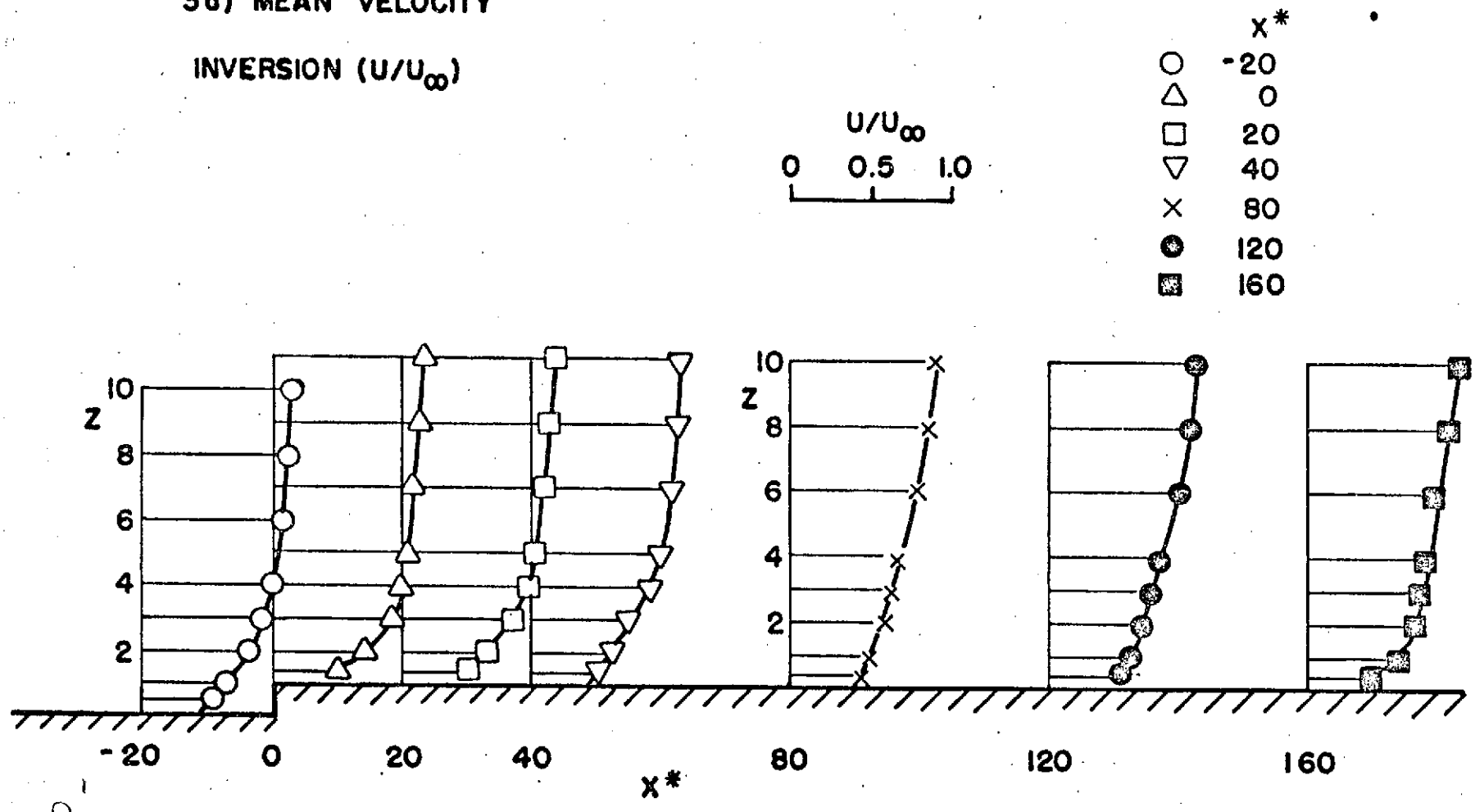

Figure 3a

3 b) MEAN TEMPERATURE

($\Delta\theta$)

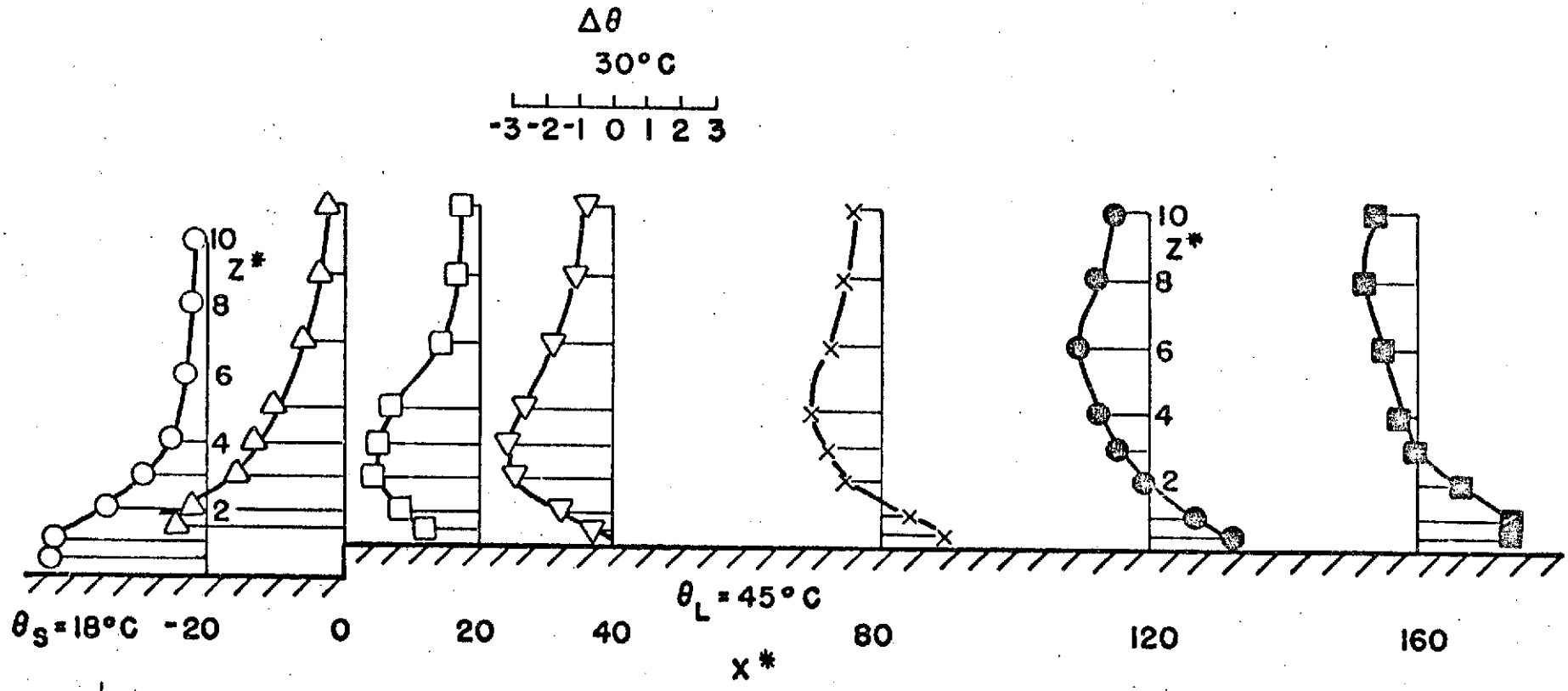

Figure 3b

3 c) RICHARDSON NUMBER

(Ri)

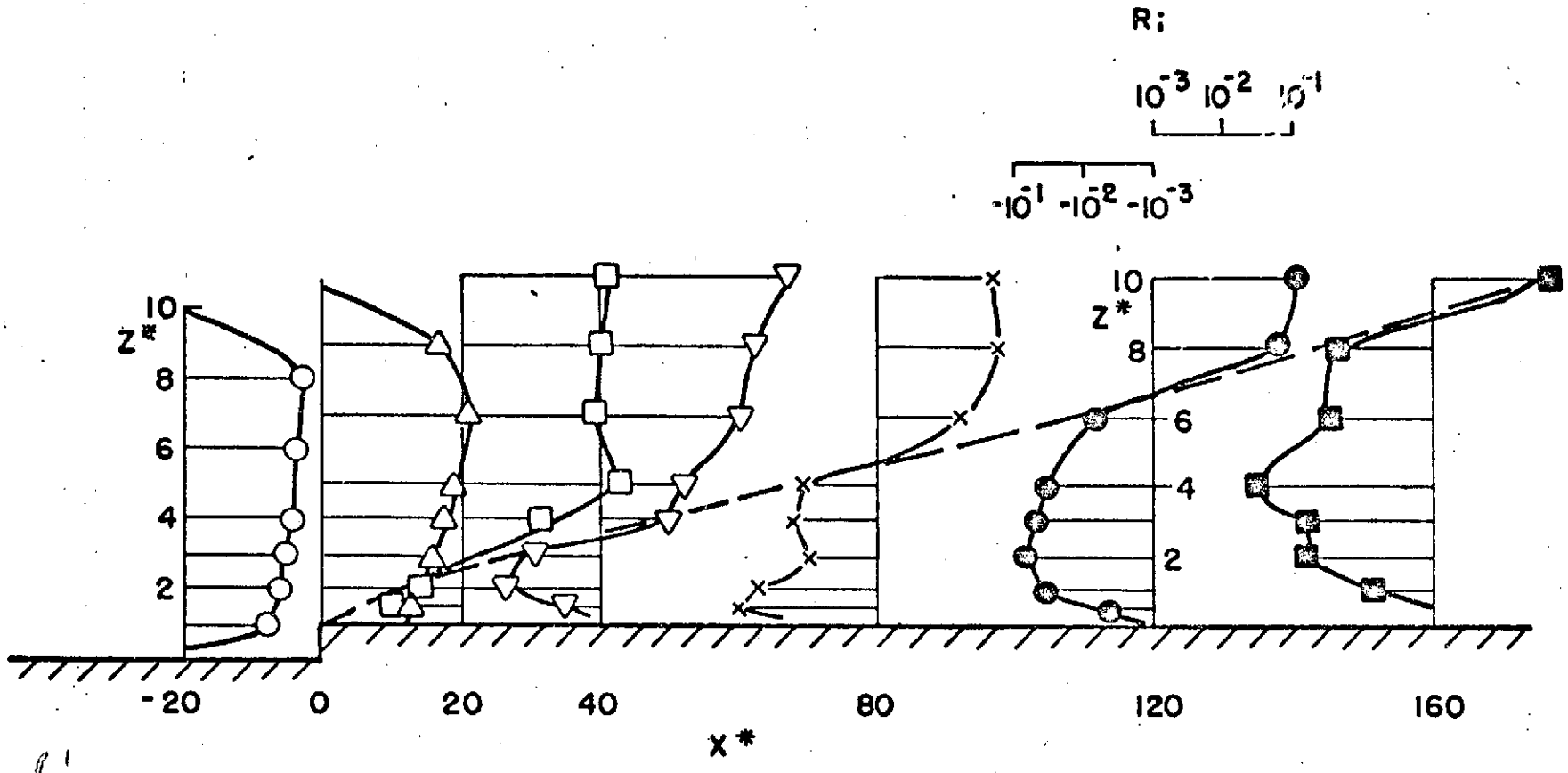

Figure 3c

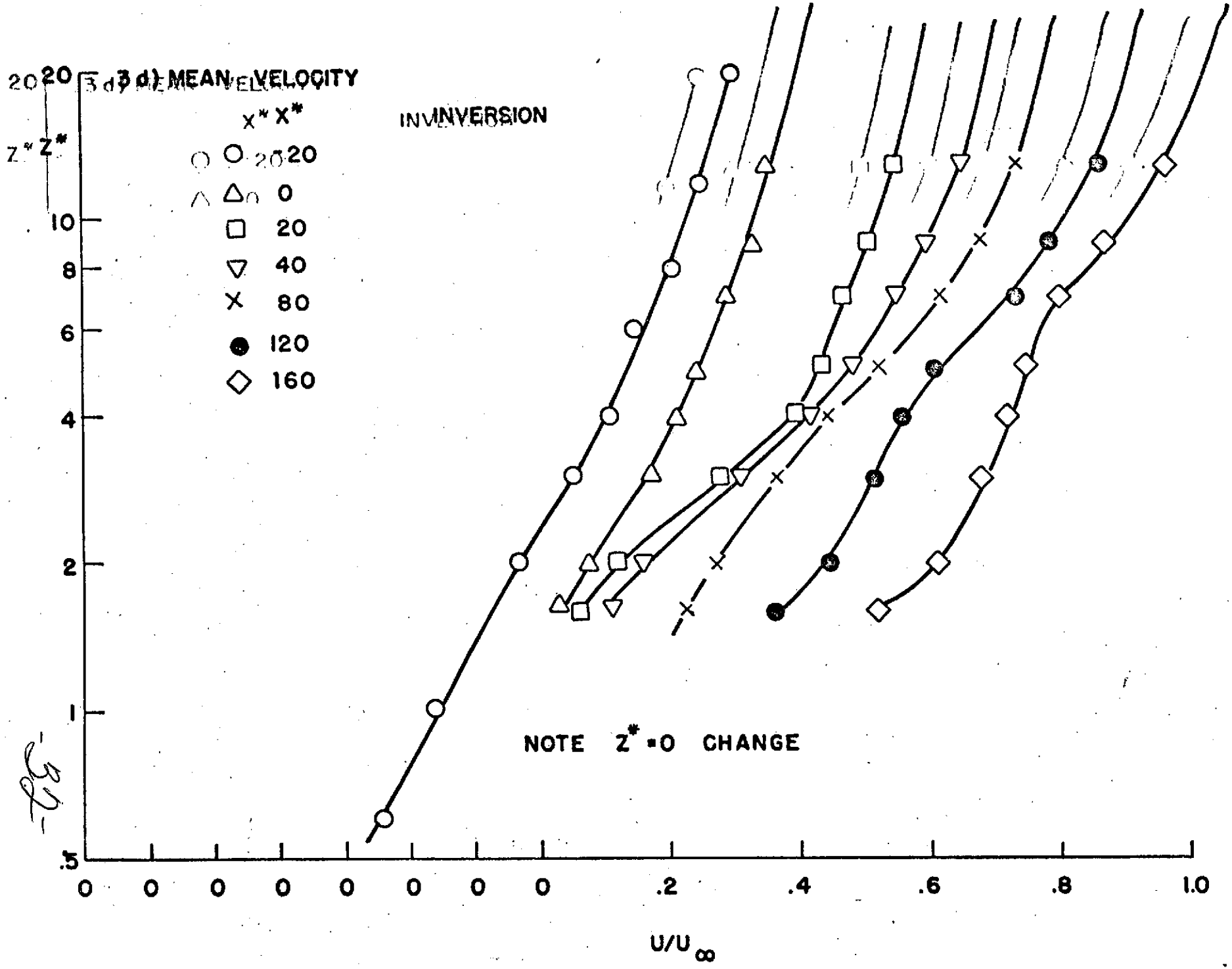
(3d) MEAN VELOCITY
INVERSION
X* X*
Z* Z*
20 20
0
20
40
80
120
160
NOTE Z* = 0 CHANGE
20
10
8
6
4
2
1
.5
0 0 0 0 0 0 0 0
.2
.4
.6
.8
1.0
U/U∞

Figure 3d

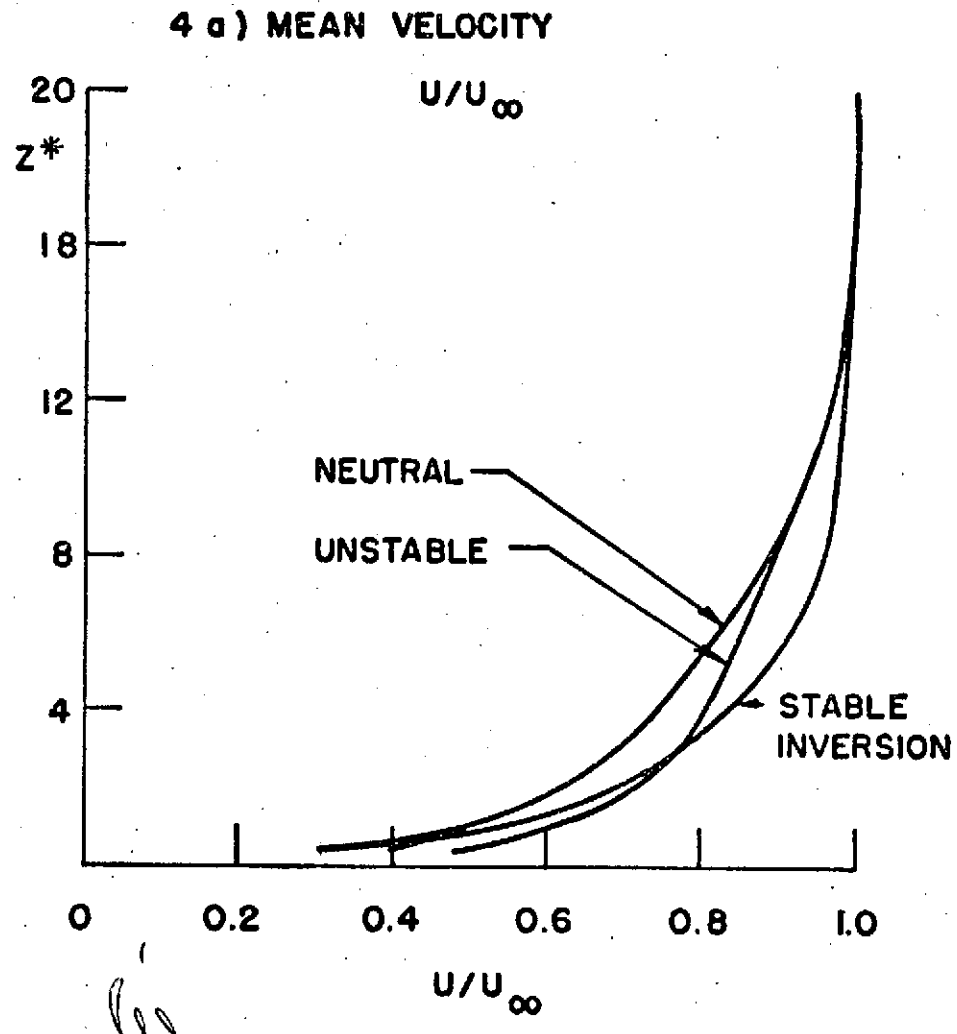
4 a) MEAN VELOCITY
U/U∞
20
Z*
18
12
8
4
NEUTRAL
UNSTABLE
STABLE
INVERSION
0
0.2
0.4
0.6
0.8
1.0
U/U∞

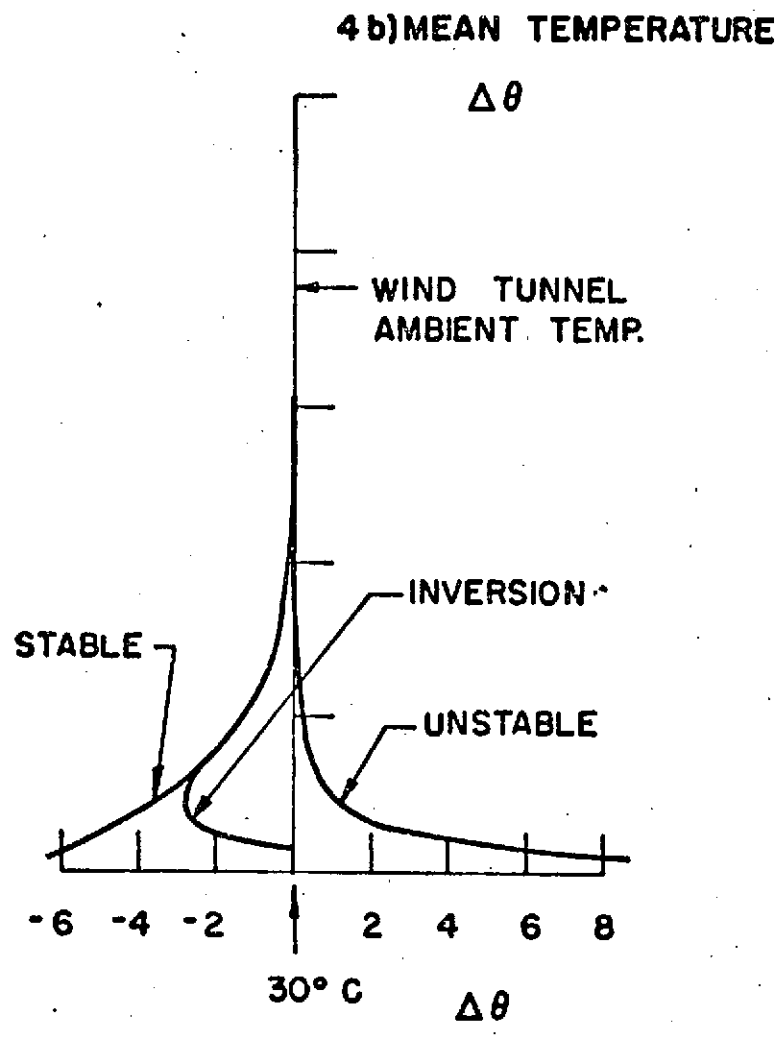
4 b) MEAN TEMPERATURE
Δθ
WIND TUNNEL
AMBIENT TEMP.
INVERSION
STABLE
UNSTABLE
-6
-4
-2
2
4
6
8
30° C
Δθ

Figure 4a, b

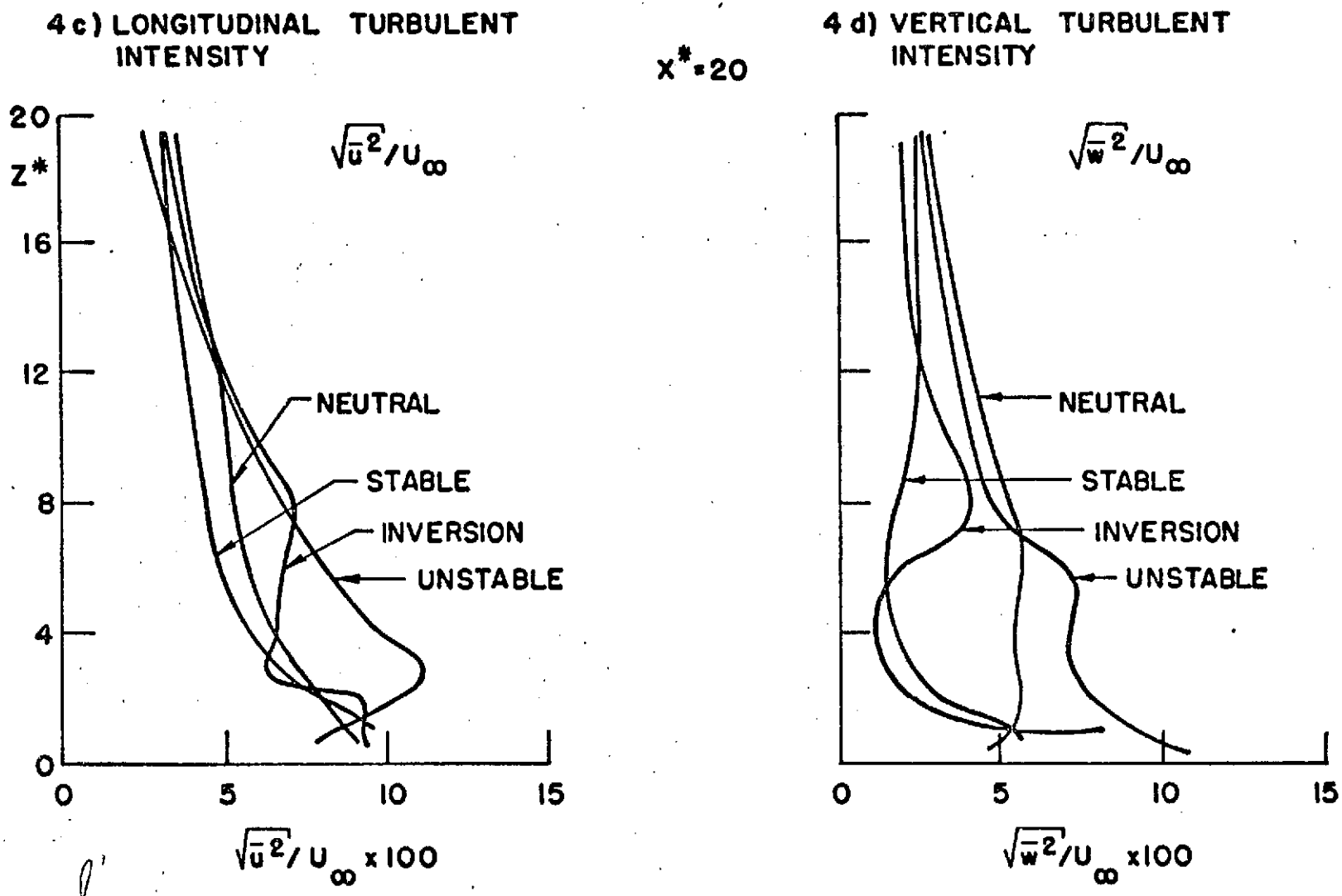
4 c) LONGITUDINAL TURBULENT INTENSITY
x*=20
20
Z*
16
12
8
4
0
$\sqrt{\overline{u}^2}/U_\infty$
NEUTRAL
STABLE
INVERSION
UNSTABLE
0
5
10
15
$\sqrt{\overline{u}^2}/U_\infty$ x100
4 d) VERTICAL TURBULENT INTENSITY
$\sqrt{\overline{w}^2}/U_\infty$
NEUTRAL
STABLE
INVERSION
UNSTABLE
0
5
10
15
$\sqrt{\overline{w}^2}/U_\infty$ x100

Figure 4c

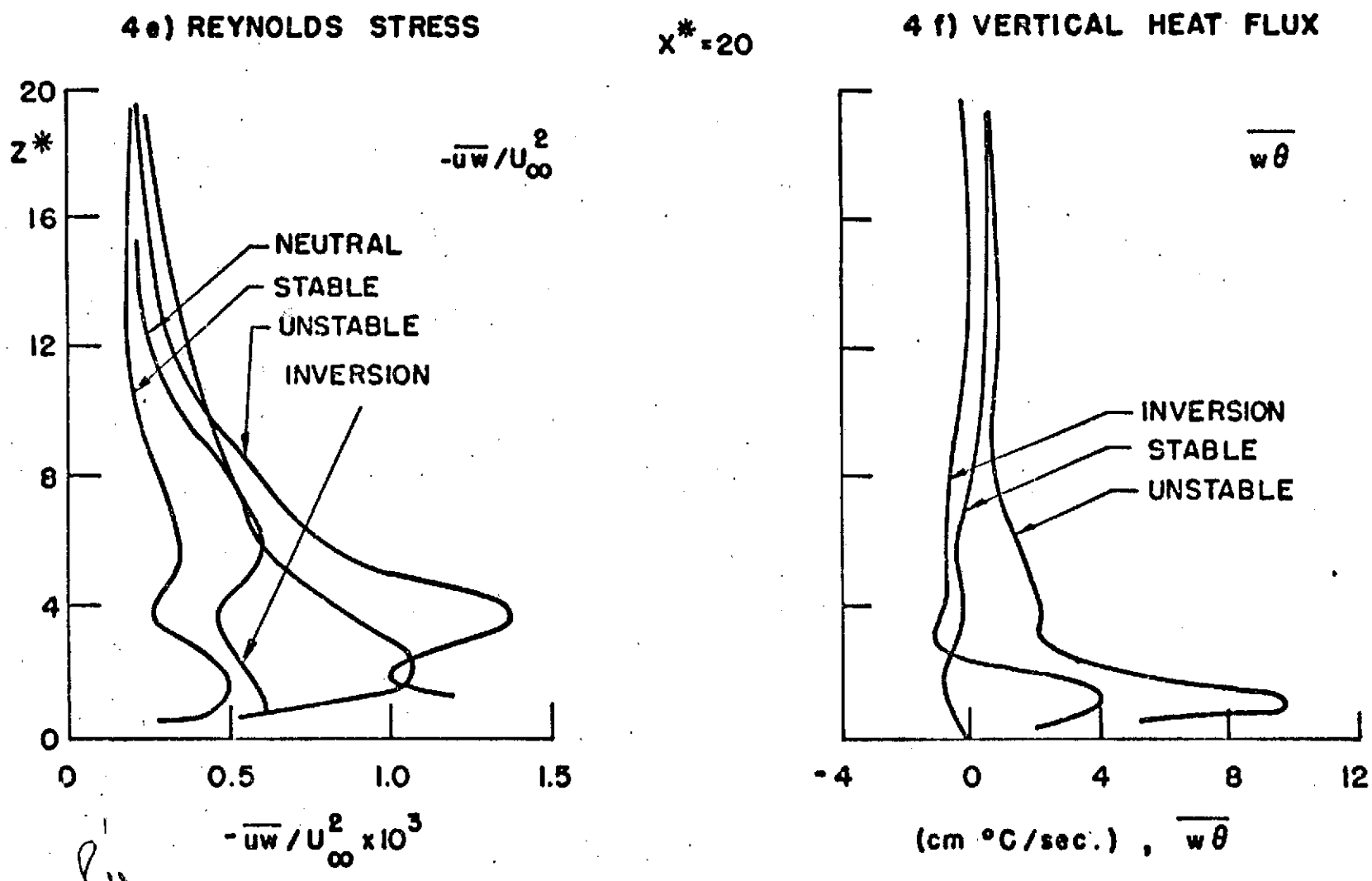
4 e) REYNOLDS STRESS
X* = 20
4 f) VERTICAL HEAT FLUX
20
Z*
16
12
8
4
0
$-\overline{uw}/U_\infty^2$
NEUTRAL
STABLE
UNSTABLE
INVERSION
0
0.5
1.0
1.5
$-\overline{uw}/U_\infty^2 \times 10^3$
$\overline{w\theta}$
INVERSION
STABLE
UNSTABLE
-4
0
4
8
12
(cm °C/sec.) , $\overline{w\theta}$

Figure 4d

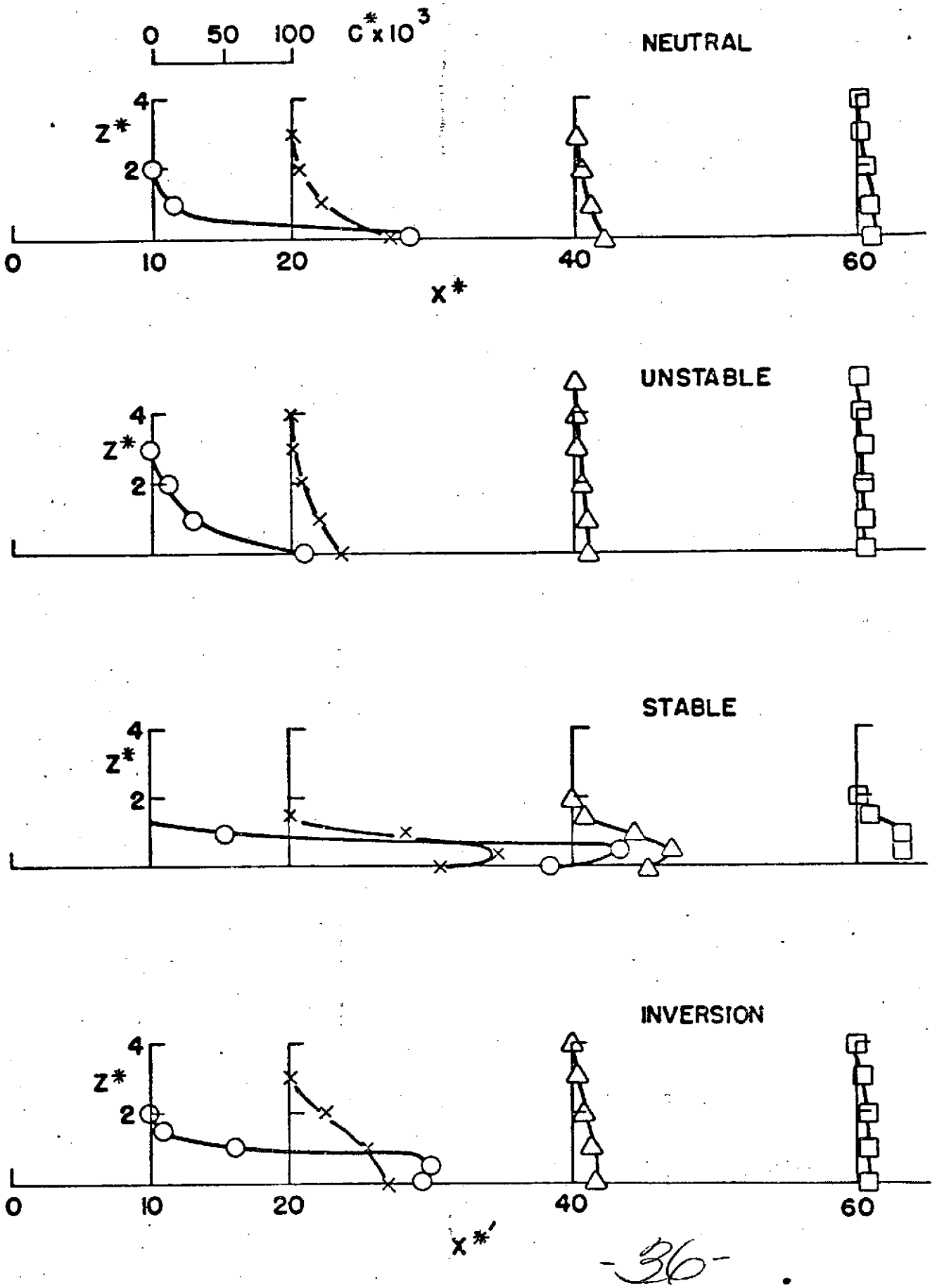
0 50 100 C*x10^3
NEUTRAL
Z*
4
2
0
10
20
40
60
X*
UNSTABLE
STABLE
INVERSION
X*'

Figure 5

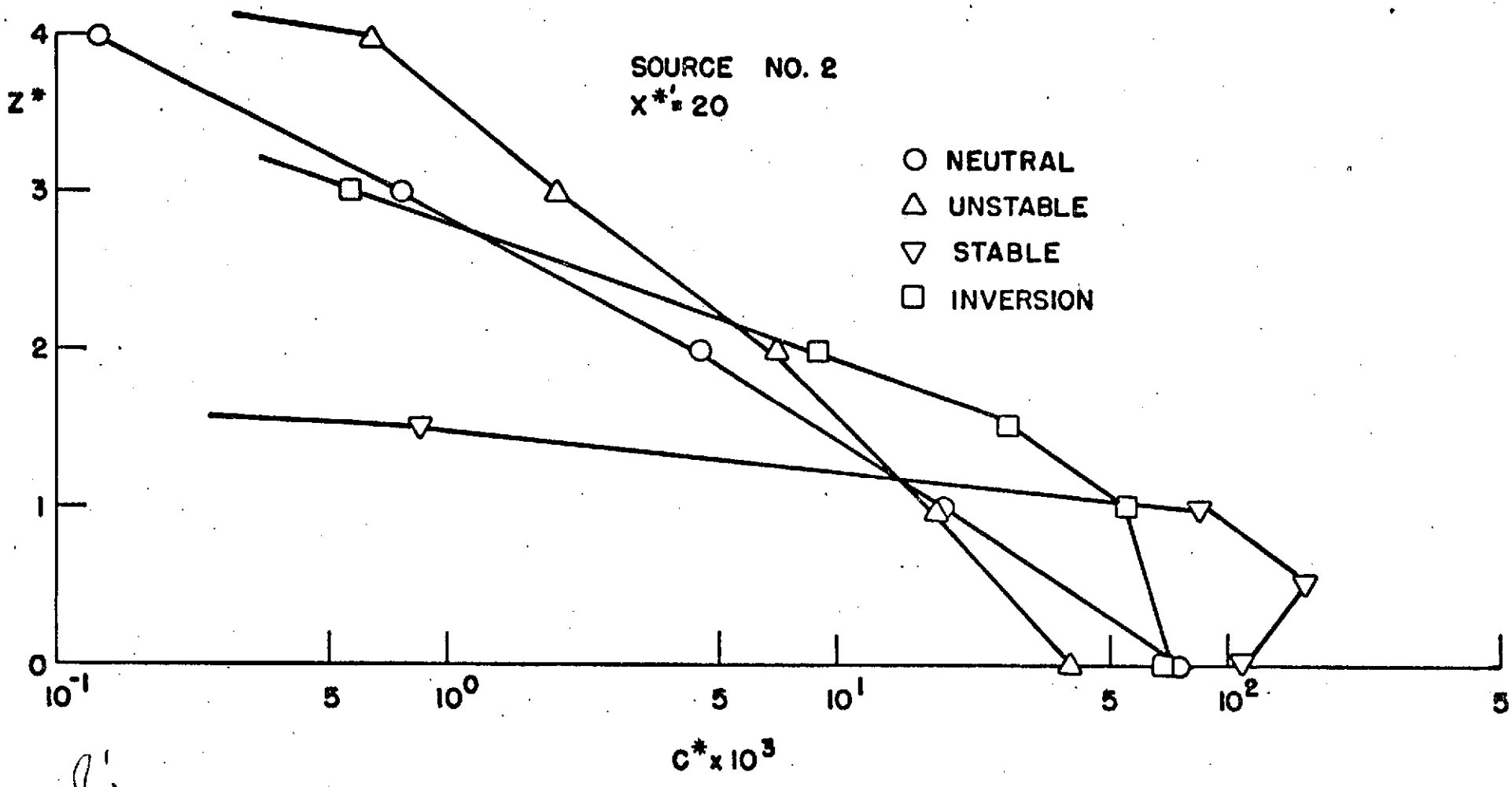
SOURCE NO. 2
X*' = 20
NEUTRAL
UNSTABLE
STABLE
INVERSION
Z*
C* x 10^3
4
3
2
1
0
10^-1
5
10^0
5
10^1
5
10^2
5

Figure 6

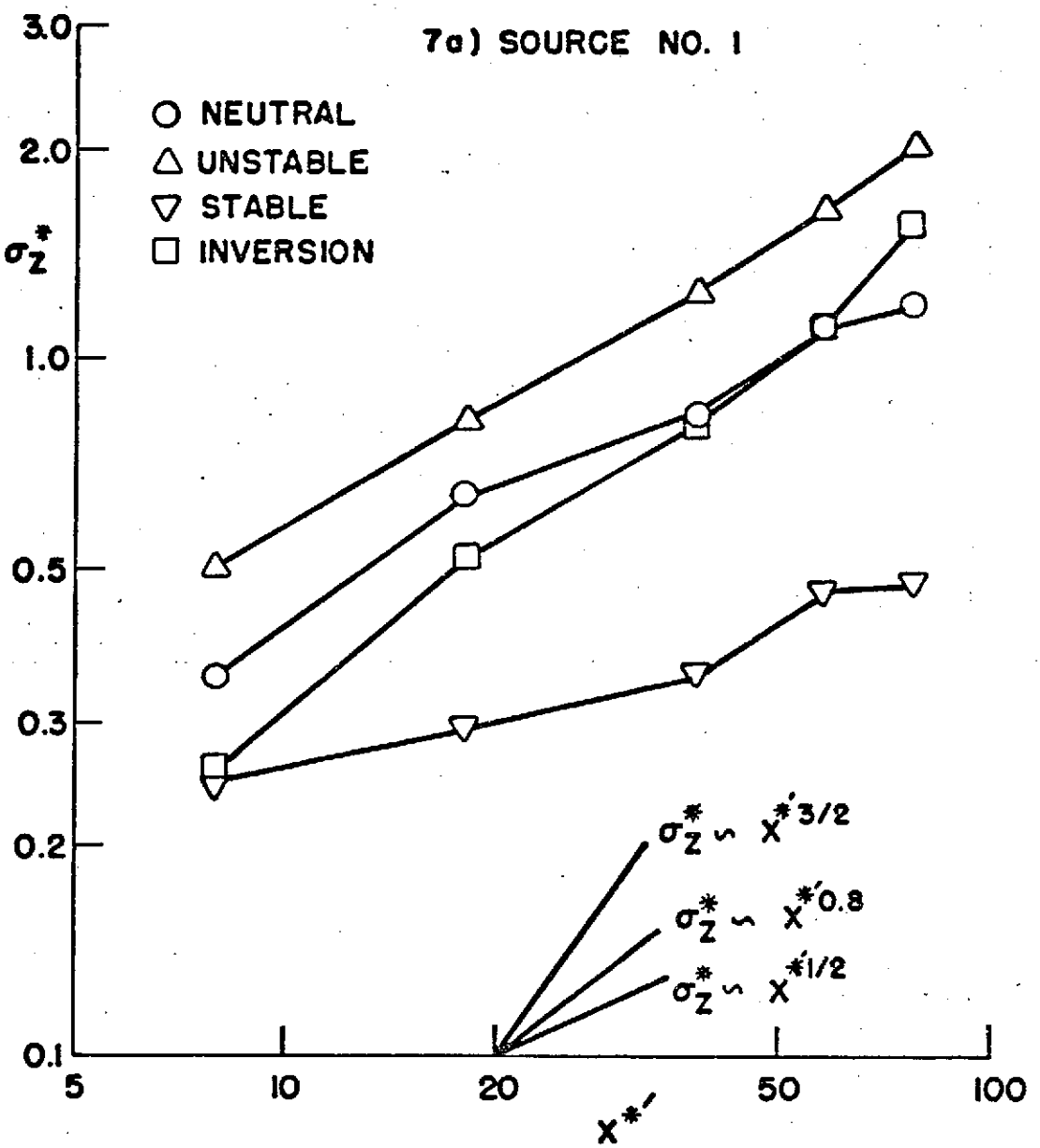
7a) SOURCE NO. 1
NEUTRAL
UNSTABLE
STABLE
INVERSION
σ_z^*
3.0
2.0
1.0
0.5
0.3
0.2
0.1
5
10
20
50
100
$X^{*\prime}$
$\sigma_z^* \sim X^{*\prime 3/2}$
$\sigma_z^* \sim X^{*\prime 0.8}$
$\sigma_z^* \sim X^{*\prime 1/2}$

Figure 7a

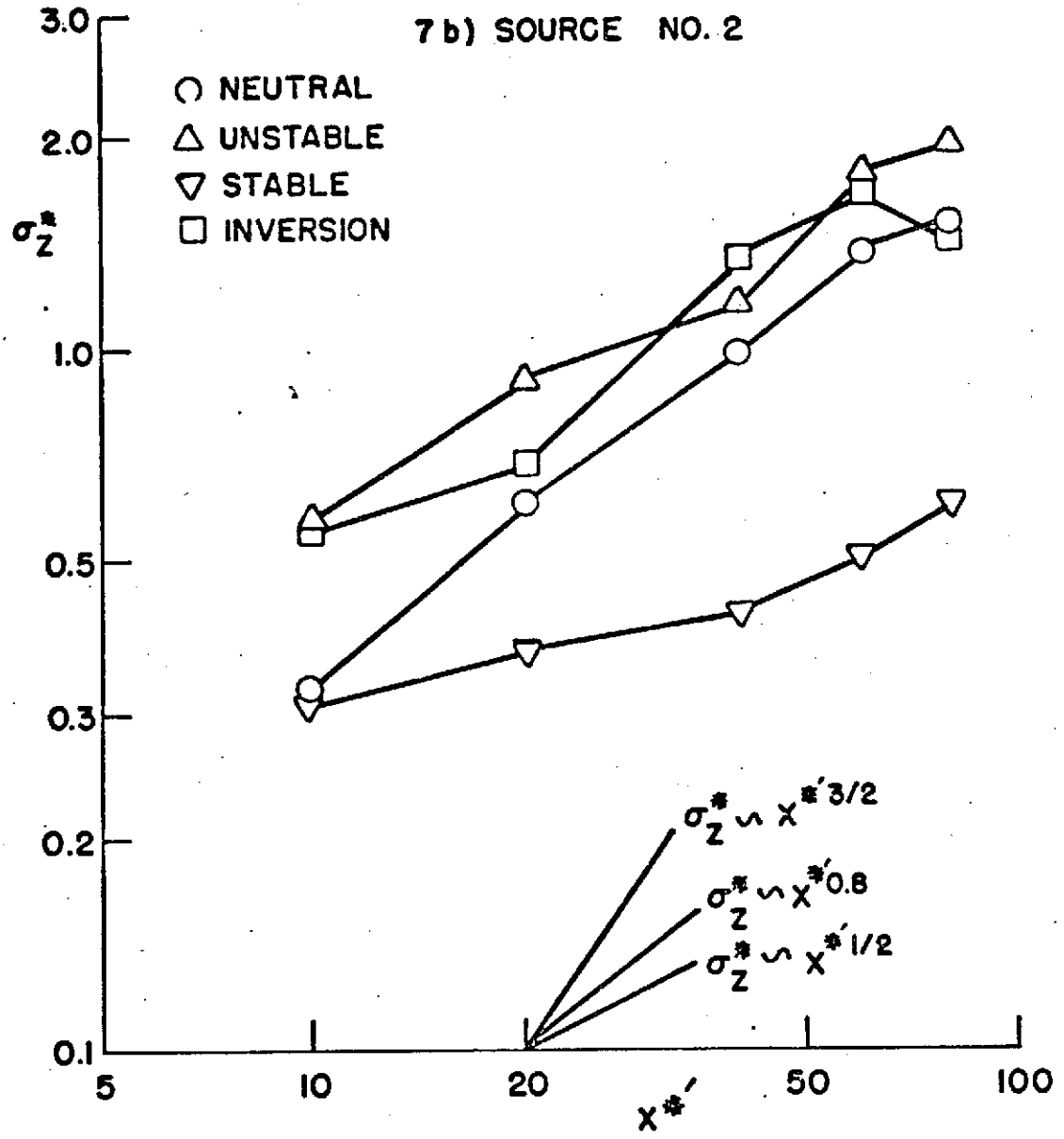
7 b) SOURCE NO. 2
NEUTRAL
UNSTABLE
STABLE
INVERSION
σ_z^*
3.0
2.0
1.0
0.5
0.3
0.2
0.1
5
10
20
50
100
$x^{*\prime}$
$\sigma_z^* \sim x^{*\prime 3/2}$
$\sigma_z^* \sim x^{*\prime 0.8}$
$\sigma_z^* \sim x^{*\prime 1/2}$

Figure 7b

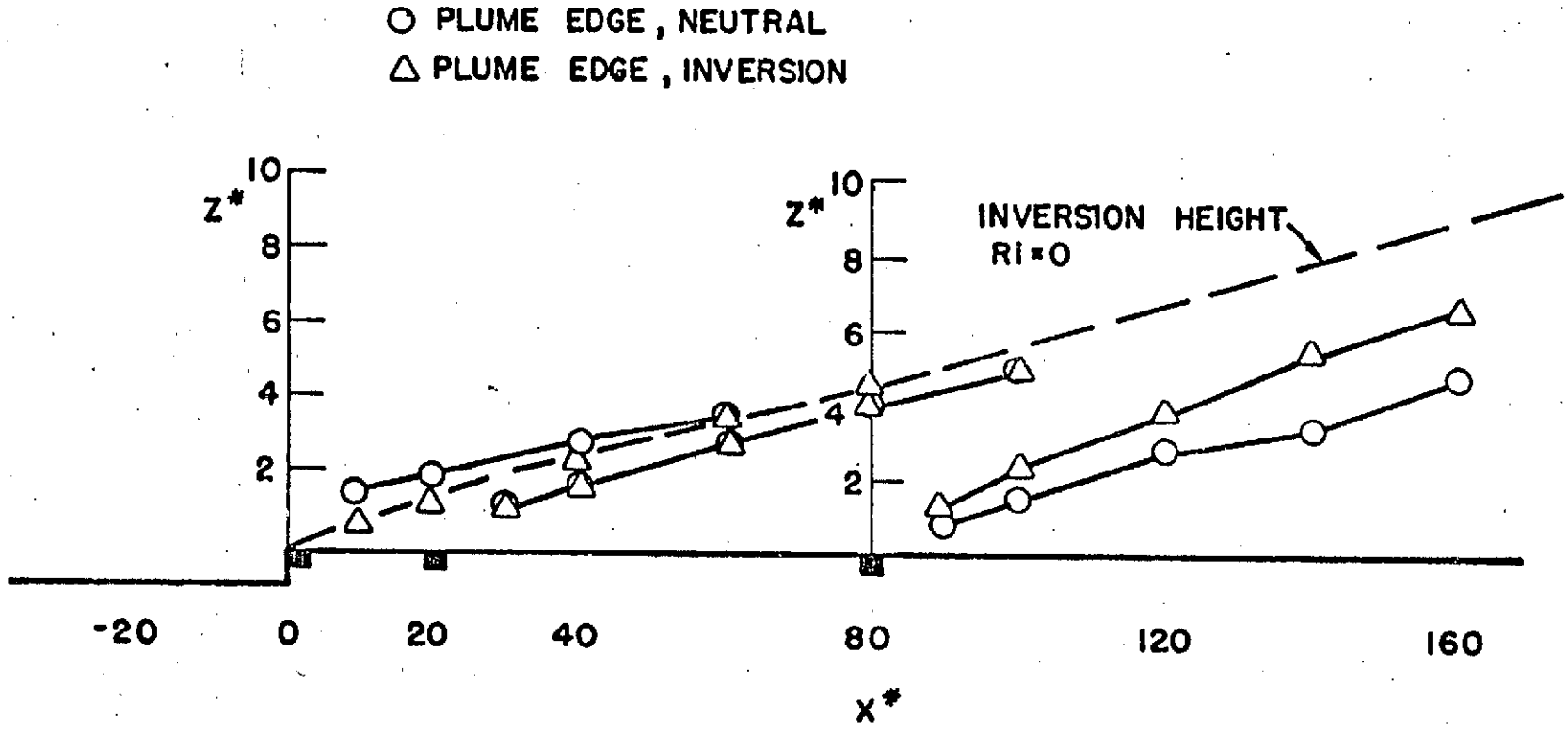
○ PLUME EDGE, NEUTRAL
△ PLUME EDGE, INVERSION
Z*
10
8
6
4
2
INVERSION HEIGHT
Ri=0
-20
0
20
40
80
120
160
X*

Figure 8

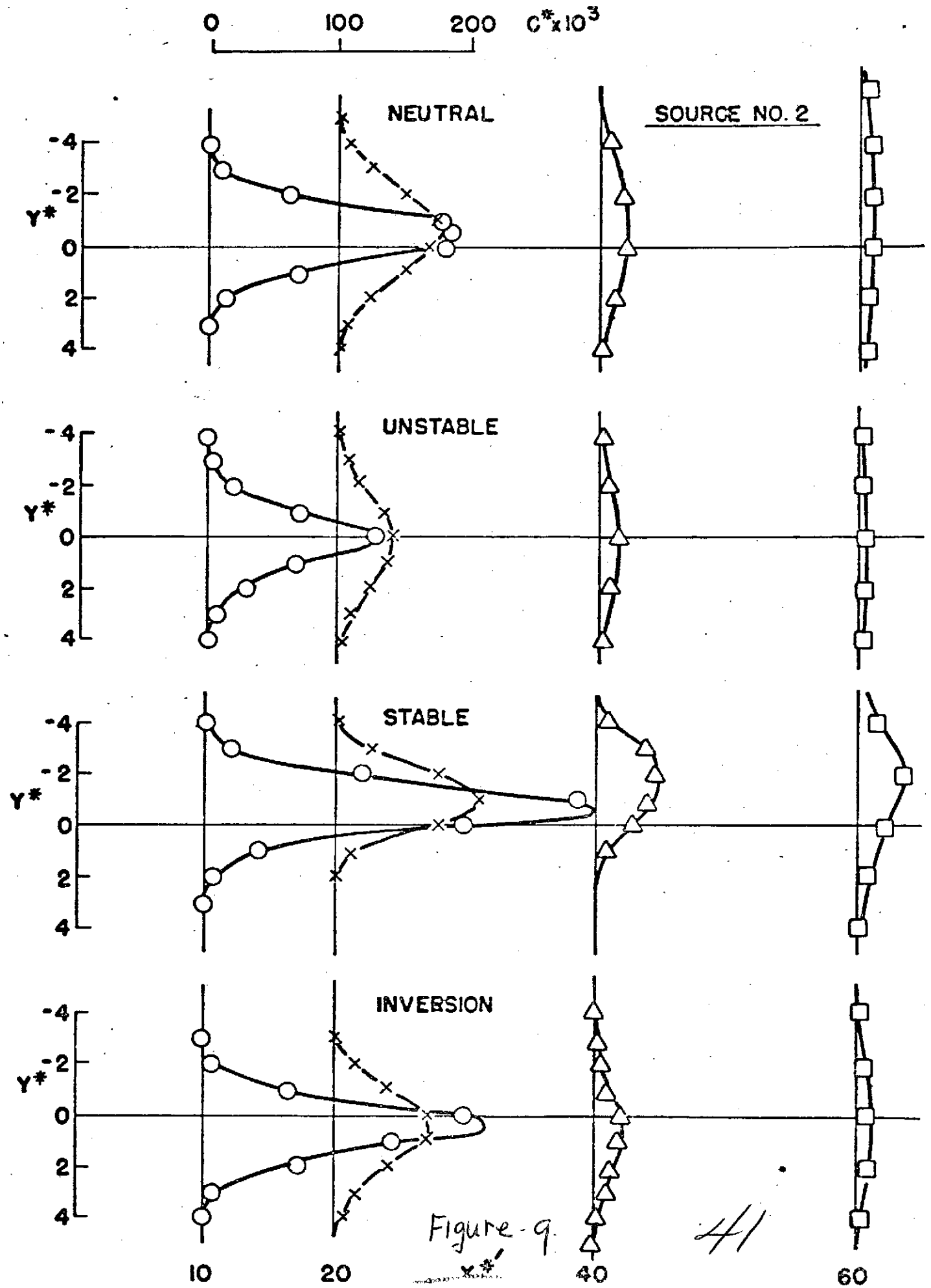
0
100
200
C*x10³
NEUTRAL
SOURCE NO. 2
UNSTABLE
STABLE
INVERSION
Y*
-4
-2
0
2
4
10
20
40
60
X*

Figure-9.

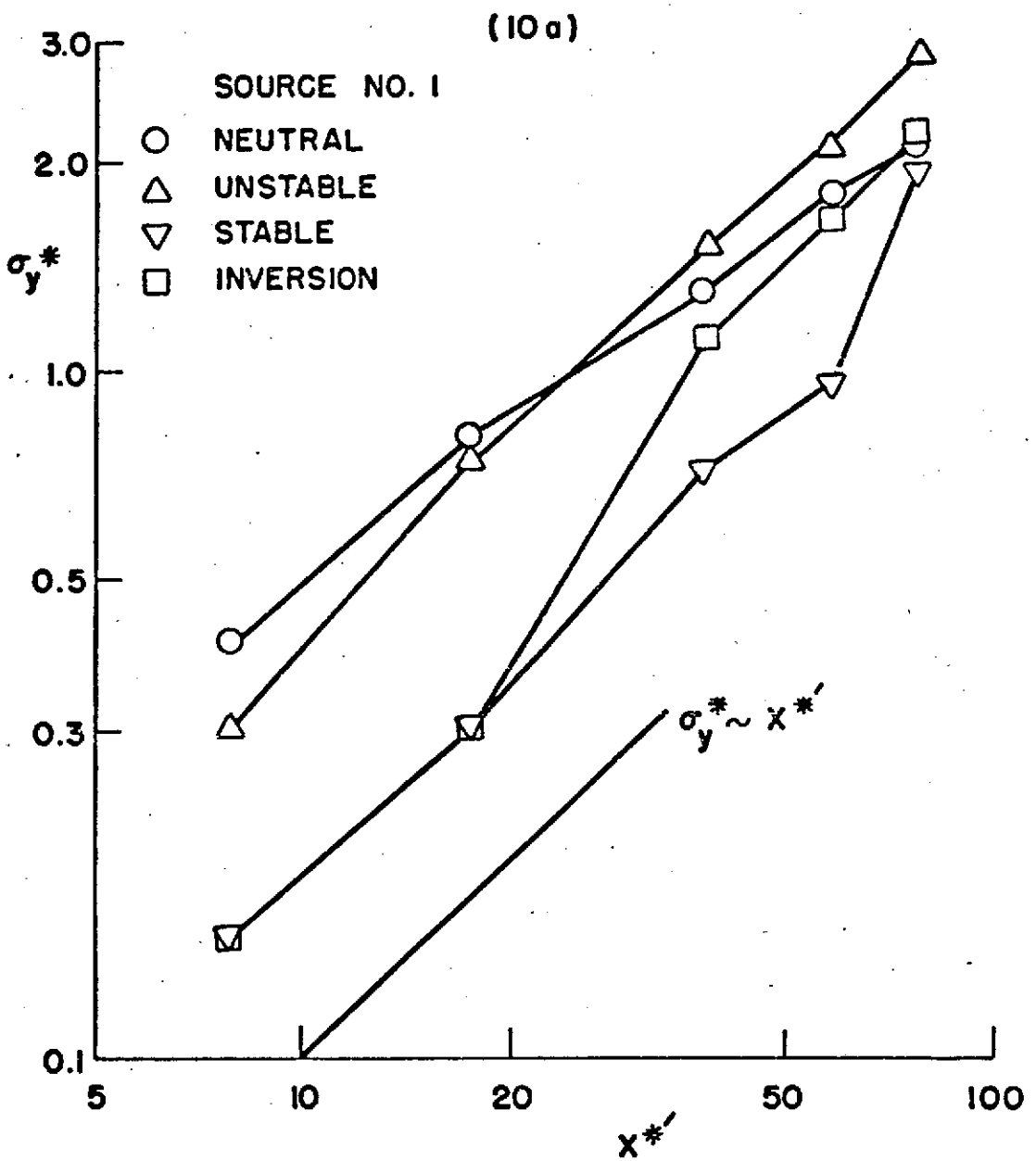
(10 a)
SOURCE NO. 1
NEUTRAL
UNSTABLE
STABLE
INVERSION
σ_y^*
3.0
2.0
1.0
0.5
0.3
0.1
5
10
20
50
100
$x^{*\prime}$
$\sigma_y^* \sim x^{*\prime}$

Figure 10a

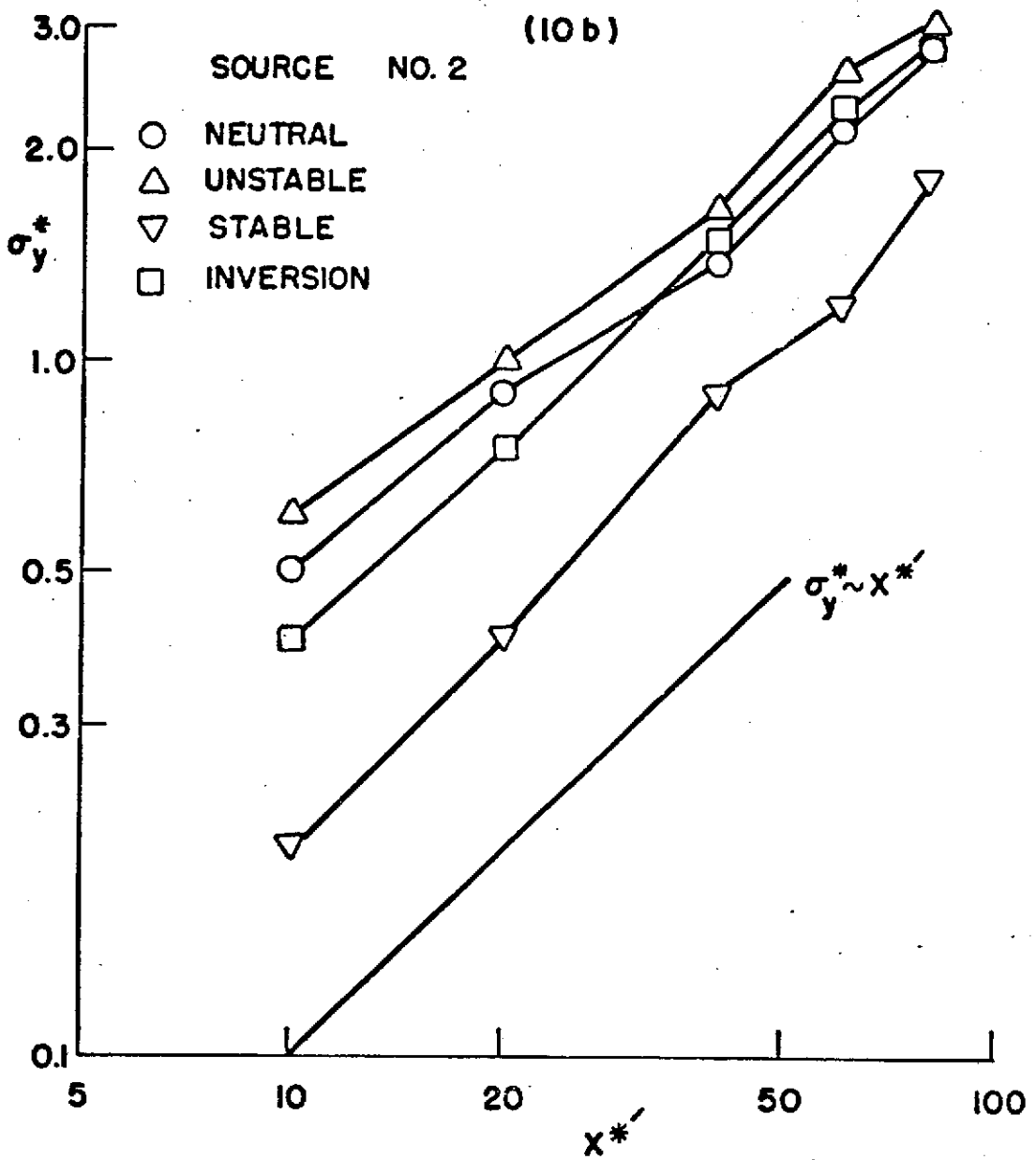
(10 b)
SOURCE NO. 2
NEUTRAL
UNSTABLE
STABLE
INVERSION
σ_y^*
3.0
2.0
1.0
0.5
0.3
0.1
5
10
20
50
100
$x^{*'}$
$\sigma_y^* \sim x^{*'}$

Figure 10b

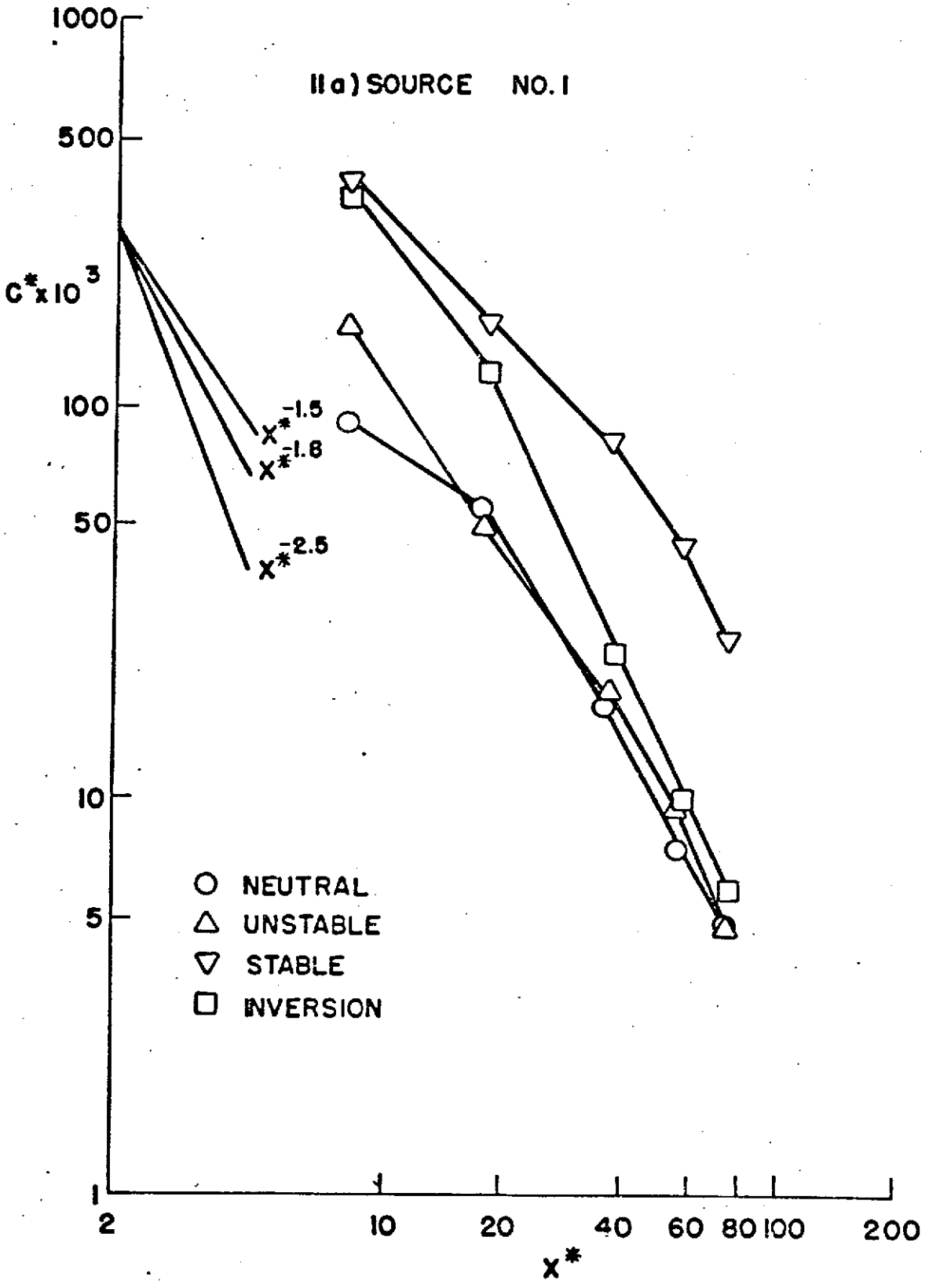
11a) SOURCE NO. 1
1000
500
100
50
10
5
1
C* x 10^3
X*^-1.5
X*^-1.8
X*^-2.5
NEUTRAL
UNSTABLE
STABLE
INVERSION
2
10
20
40
60
80
100
200
X*

Figure 11a

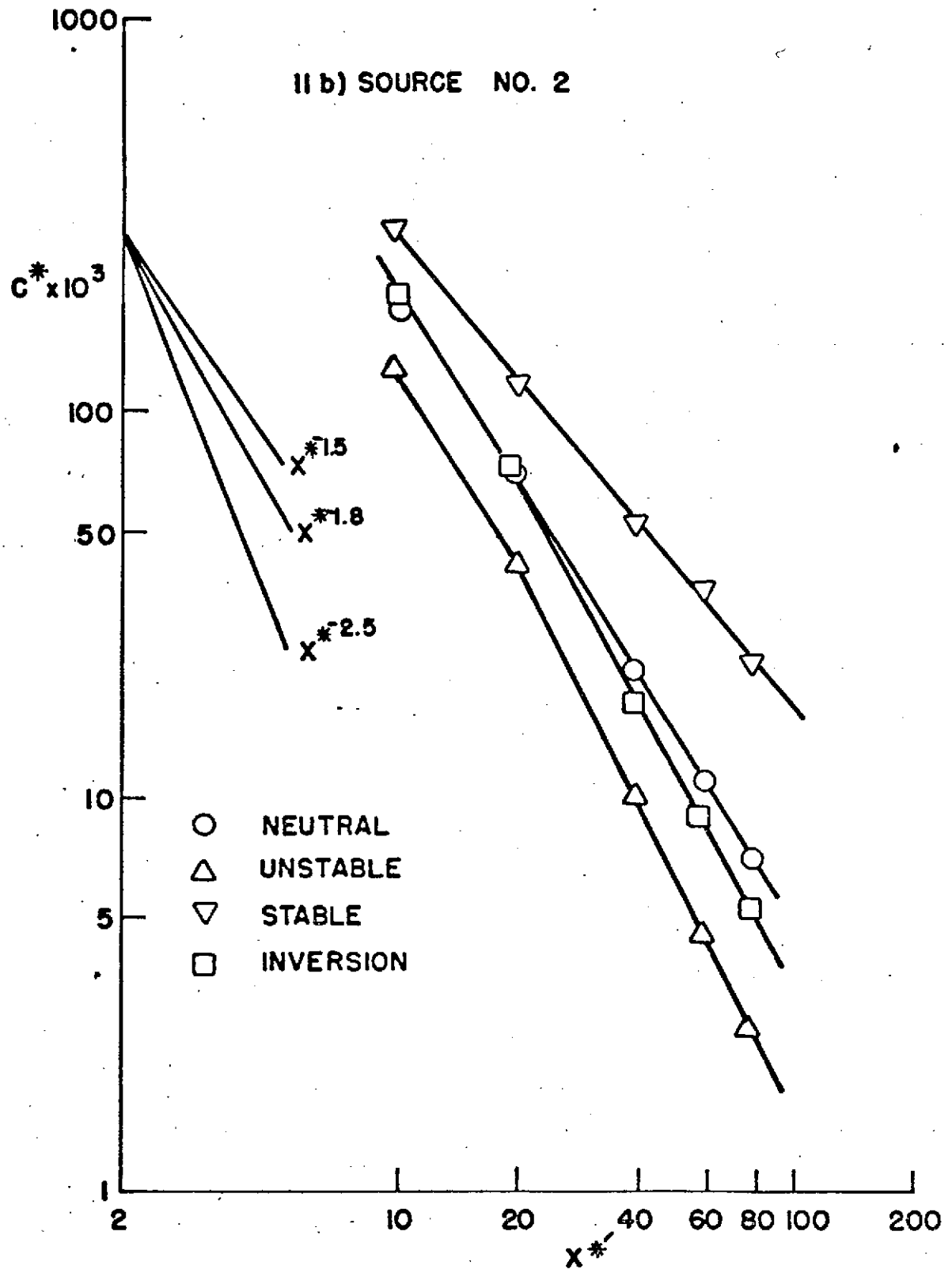
11 b) SOURCE NO. 2
1000
100
50
10
5
1
C* x 10^3
X*1.5
X*1.8
X*2.5
NEUTRAL
UNSTABLE
STABLE
INVERSION
2
10
20
40
60
80
100
200
X*

Figure 11b

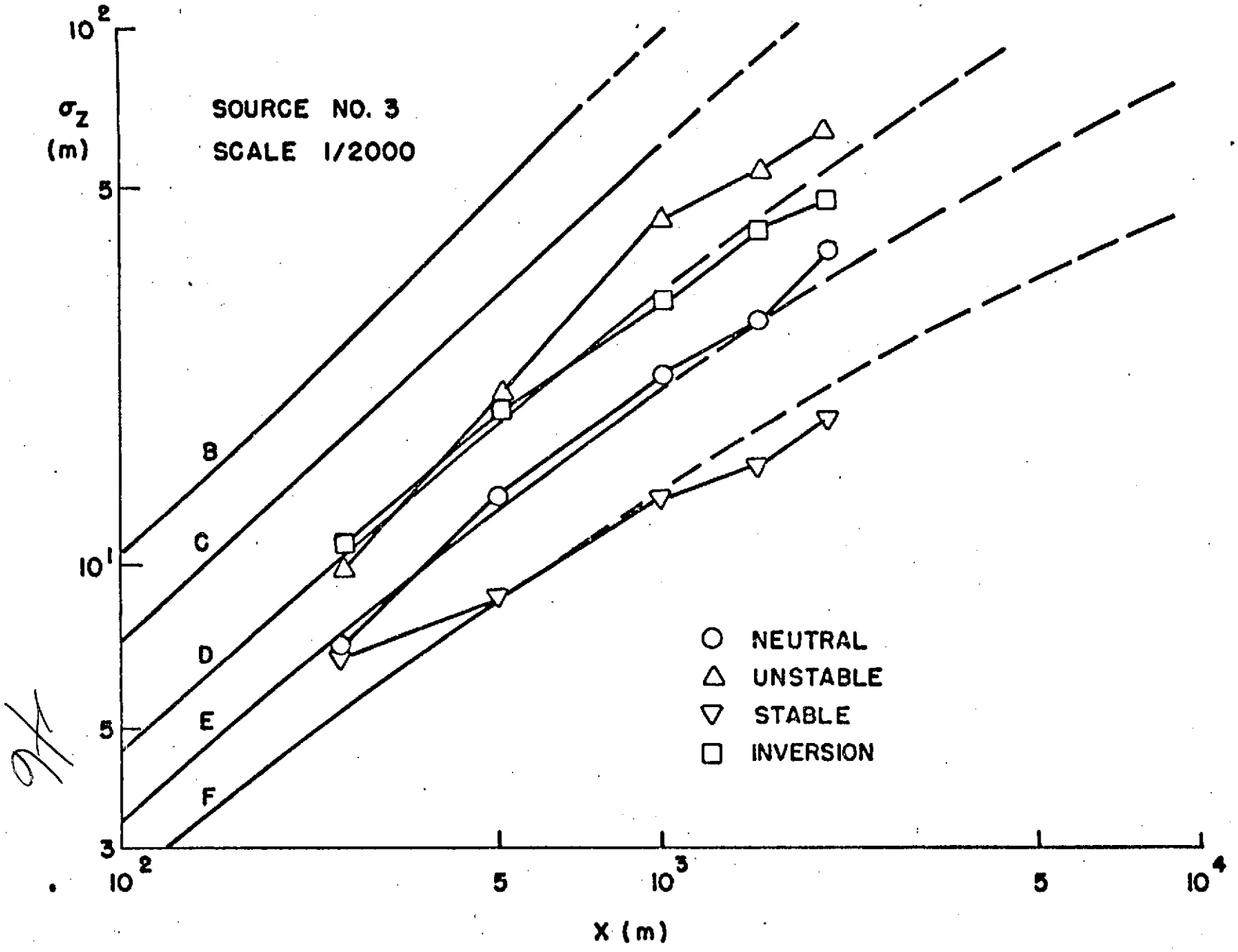
SOURCE NO. 3
SCALE 1/2000
σ_z (m)
10^2
5
10^1
5
3
B
C
D
E
F
NEUTRAL
UNSTABLE
STABLE
INVERSION
10^2
5
10^3
5
10^4
X (m)

Figure 12

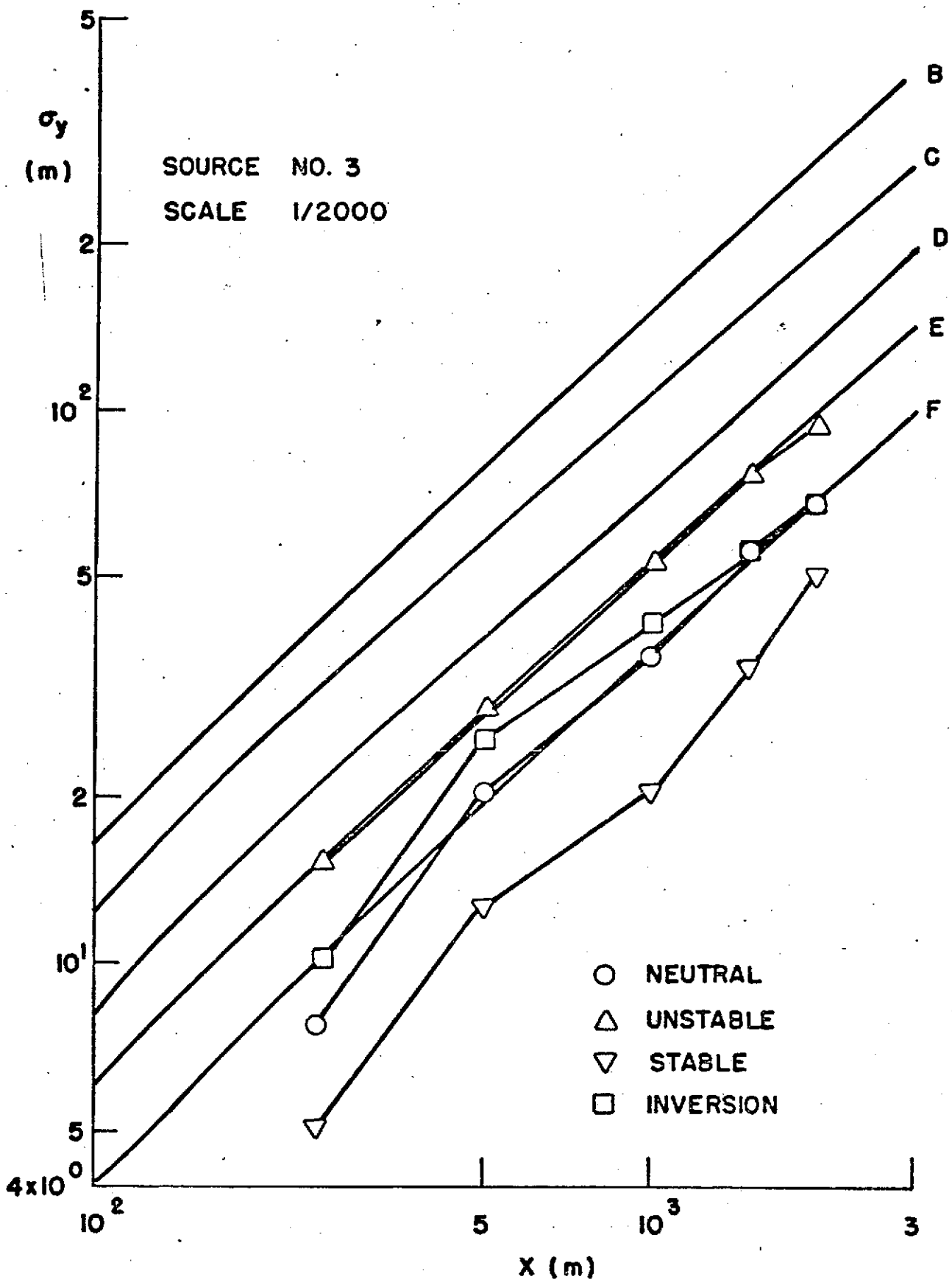
σy
(m)
SOURCE NO. 3
SCALE 1/2000
B
C
D
E
F
5
2
10²
5
2
10¹
5
4x10⁰
10²
5
10³
3
X (m)
NEUTRAL
UNSTABLE
STABLE
INVERSION

-47-

Figure 13

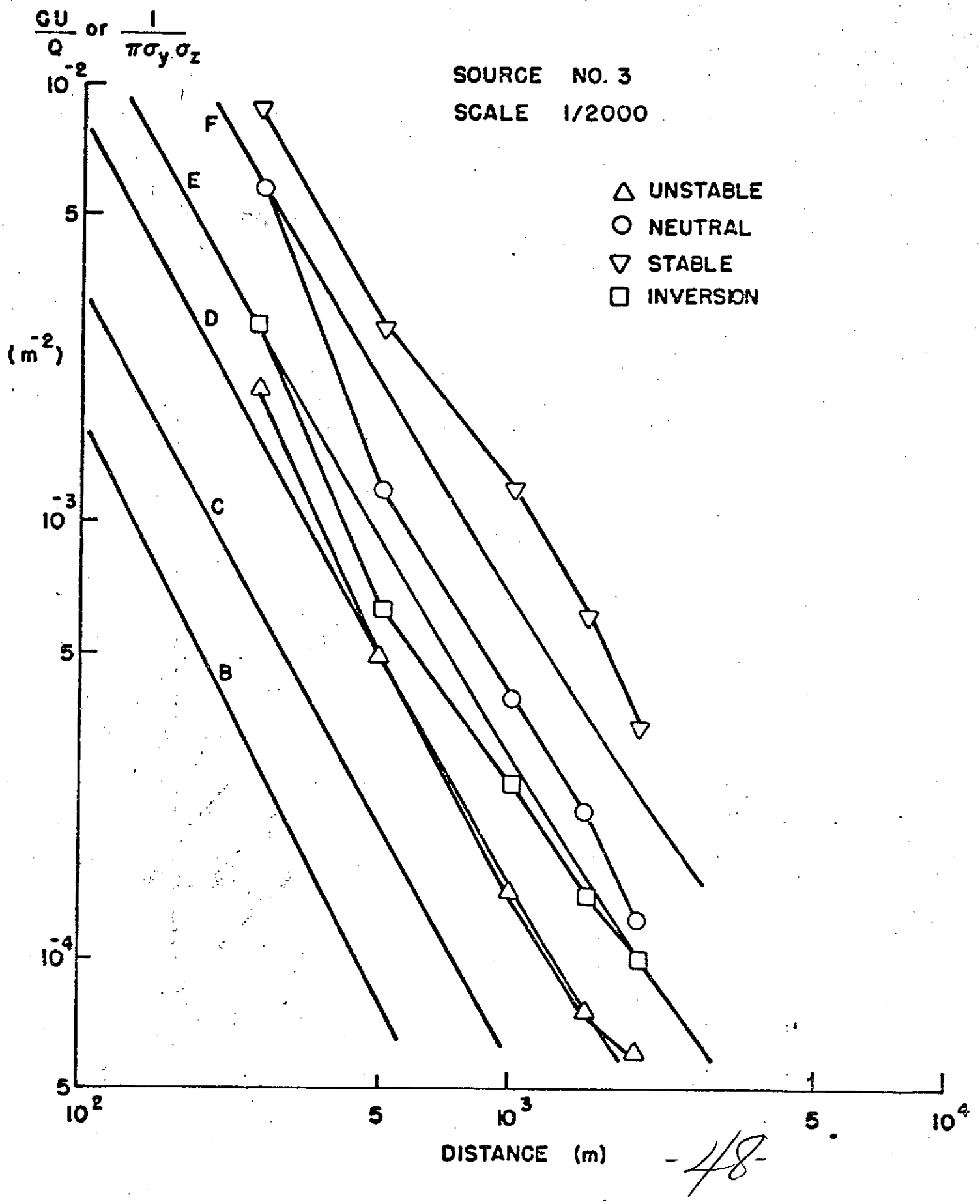
GU/Q or 1/πσyσz
SOURCE NO. 3
SCALE 1/2000
△ UNSTABLE
○ NEUTRAL
▽ STABLE
□ INVERSION
F
E
D
C
B
(m⁻²)
10⁻²
5
10⁻³
5
10⁻⁴
5
10²
5
10³
1
5
10⁴
DISTANCE (m)

Figure 14